

Tests of Electron Flavor Conservation with the Sudbury Neutrino Observatory

John N. Bahcall

Institute for Advanced Study, Princeton, New Jersey 08540

Eligio Lisi

*Institute for Advanced Study, Princeton, New Jersey 08540
and Istituto Nazionale di Fisica Nucleare, Sezione di Bari, Italy*

Abstract

We analyze tests of electron flavor conservation that can be performed at the Sudbury Neutrino Observatory (SNO). These tests, which utilize ^8B solar neutrinos interacting with deuterium, measure: 1) the shape of the recoil electron spectrum in charged-current (CC) interactions (the CC spectrum shape); and 2) the ratio of the number of charged current to neutral current (NC) events (the CC/NC ratio). We determine standard model predictions for the CC spectral shape and for the CC/NC ratio, together with realistic estimates of their errors and the correlations between errors. We consider systematic uncertainties in the standard neutrino spectrum and in the charged-current and neutral current cross-sections, the SNO energy resolution and absolute energy scale, and the SNO detection efficiencies. Assuming that either matter-enhanced or vacuum neutrino oscillations solve the solar neutrino problems, we calculate the confidence levels with which electron flavor non-conservation can be detected using either the CC spectrum shape or the CC/NC ratio, or both. If the SNO detector works as expected, the neutrino oscillation solutions that best-fit the results of the four operating solar neutrino experiments can be distinguished unambiguously from the standard predictions of electron flavor conservation.

PACS number(s): 11.30.Fs, 26.65.+t, 13.15.+g, 12.60.-i

I. INTRODUCTION

We assess quantitatively the possibility of detecting electron flavor non-conservation using ^8B solar neutrino interactions in deuterium at the Sudbury Neutrino Observatory (SNO) [1]. The separate conservation of the lepton (electron, muon, tau) flavors is a well known ingredient of the standard electroweak model [2] and of some of its extensions.

Figures 7 and 8 (and Table I and Table II) summarize the power of the SNO experiment to find new physics. We urge the reader to look at these two summary figures (and tables) before descending into the necessary details, which are analyzed in this paper.

Solar neutrinos offer a unique possibility to detect electron-flavor non-conserving processes. In solar neutrino experiments, a pure beam of electron neutrinos is created in the interior of the sun, passing through 10^{11} gm cm^{-2} of matter and eventually reaching a terrestrial detector located at a distance of 10^8 km from the sun. The tests discussed in this paper are independent of solar models and are made possible by the fact that low energy (MeV) nuclear fusion reactions produce only electron type neutrinos. For neutrino squared mass differences less than 10^{-4} eV², the solar neutrino tests are more sensitive than laboratory tests [3] of lepton flavor conservation.

We consider measurements of: 1) the energy spectrum of recoil electrons in charged current (absorption) reactions [4]; 2) the ratio of the number of charged-to-neutral current events [5]; and 3) the combined measurement of the charged current energy spectrum and the charged to neutral current ratio. The shape measurement is sensitive to an energy-dependent depletion of the created flux of electron flavor neutrinos, and the neutral current to charged current comparison is sensitive to a non-zero conversion probability to a different (active) neutrino.

How can we test lepton flavor conservation with solar neutrinos? The energy spectrum of ^8B neutrinos is the same in the laboratory and in the sun, modulo negligible (gravitational redshift) corrections of $\mathcal{O}(10^{-5})$ [4]. Fortunately, the spectrum, $\lambda(E_\nu)$, can be determined with relatively small uncertainties from laboratory data on the $^8\text{B}(\beta^+)^8\text{Be}(2\alpha)$ decay chain [6]. The measurement of the electron spectrum produced by neutrino absorption is therefore a test for new physics independent of complications related to solar physics. The ratio of neutral current to charged current events is also independent of uncertainties that affect the calculation of the total flux.¹ All of the observed solar neutrinos must be of the electron type unless the separate conservation of electron flavor is violated.

Neutrino oscillations are used in this paper to illustrate the potential effects of flavor transitions, but the considerations described here can be applied to other proposed electron-flavor non-conserving mechanisms, such as neutrino decay [7,8], non-standard electromagnetic properties [9–11], neutrino violation of the equivalence principle [12], and supersymmetric flavor-changing neutral currents [13,14]. Many of the key papers and other relevant references are reprinted in [15].

Will the measurements with SNO be sensitive enough to prove—if it is present—that new

¹The calculated total flux of ^8B neutrinos at earth (all flavors) depends on solar physics and on the extrapolated low-energy cross section for the reaction $^7\text{Be}(p, \gamma)^8\text{B}$.

neutrino physics is occurring? Will the uncertainties (systematic and statistical) be sufficiently small to identify electron flavor non-conservation if it occurs as previously suggested? The answer is: “Yes, if SNO performs as expected” [1].

The SNO collaboration is completing the construction of a 1000 ton deuterium detector in the Creighton Mine (Walden, Canada) [16]. The detector will measure the rates of the charged (CC) and neutral (NC) current reactions induced by solar neutrinos in deuterium:

$$\nu_e + d \rightarrow p + p + e^- \quad (\text{CC absorption}) \quad , \quad (1)$$

$$\nu_x + d \rightarrow p + n + \nu_x \quad (\text{NC dissociation}) \quad , \quad (2)$$

including the determination of the electron recoil energy in Eq. (1). Only the more energetic ^8B solar neutrinos will be detected² since the expected SNO threshold for CC events is an electron kinetic energy of about 5 MeV and the physical threshold for NC dissociation is the binding energy of the deuteron, $E_b = 2.225$ MeV.

Neglecting all systematic uncertainties, some previous authors [1,18–20] have considered how well the tests of flavor conservation by SNO can discriminate between new neutrino physics scenarios and standard model expectations. The most explicit discussions are given in [19] and [20], which constitute especially good introductions to the subject. We evaluate the effects of systematic uncertainties, theoretical and experimental, on the discriminatory power of the SNO tests for new physics. We consider uncertainties related to the laboratory shape of the neutrino energy spectrum, the calculated cross sections for charged-current and neutral-current reactions with deuterium, the energy calibration and resolution, detection efficiencies, and the CC detection threshold of the SNO detector.

The primary goal of this paper is to refine the best-estimates and uncertainties for the theoretical ingredients that will determine how powerfully SNO will test electron flavor conservation. In addition, we carry out a preliminary overall estimate of the sensitivity of the detector to different types of oscillation phenomena, including realistic estimates of the experimental characteristics and their uncertainties. The various backgrounds [1] will not be known until after the detector is operating and are not included here.

Our analysis is not a substitute for the detailed Monte Carlo simulations of the operating detector which will be performed by the SNO team. The discriminatory power of the detector will be established definitively by the simulations to be performed by the SNO collaboration, which will include all the theoretical ingredients discussed here, the detector elements that we high-light, and other aspects of the detector (such as the backgrounds) that will be determined during the operation of the experiment. Our calculations can, however, be a useful guide as to what is likely to be possible and what uncertainties are most important to try to reduce. We note that the SNO collaboration has been working for a number of years to develop the detector and calibration techniques in ways that will minimize the experimental uncertainties.

We shall show that the recognized systematic uncertainties permit the observation of new physics at SNO, but the systematic errors may well dominate the total uncertainties

² The contribution of *hep* neutrinos [17] is negligible and will be discussed in Sec. II A.

after a relatively short exposure (~ 1 year) to solar neutrinos. Our analysis can be extended easily to include additional sources of uncertainties.

We concentrate here on the most direct tests for new physics, which involve the shape of the neutrino spectrum and the charged-current to neutral-current ratio. If SNO does find evidence for new physics, the next step will be to discriminate among competing models of new physics. Important information will be provided by the time-dependence of the observed solar neutrino signal (day-night and seasonal variations) [1]. We do not address questions related to the time-dependence in this paper.

The SNO collaboration plans an overall test of the detector by measuring the energy spectrum of an intense ^8Li beta-decay source to be placed in the SNO detector [21]. We include in Appendix A our determination, using the best-available data, of the $^8\text{Li}(\beta)$ spectrum, together with its estimated uncertainties. We also discuss some possible strategies for the ^8Li -test.

This paper has the following structure. In Sec. II, we describe the neutrino-related ingredients of our calculation: the ^8B neutrino energy spectrum, and the charged and neutral current neutrino cross sections for deuterium. In Sec. III, we discuss the detector-related ingredients: the energy resolution, the absolute energy scale, the detection efficiencies, and the CC energy threshold. We use in Sec. IV the neutrino-related and the detector-related ingredients to calculate the flavor-conserving expectations for the shape of the CC electron recoil energy spectrum and the CC/NC event ratio; we include realistic estimates of the likely uncertainties and the correlations among the uncertainties. In Sec. V, we calculate the effects upon measurable quantities of representative neutrino oscillation scenarios, and assess quantitatively the statistical significance with which new physics might be observed. We summarize our work in Sec. VI. Appendix A presents a calculation and discussion of the $^8\text{Li}(\beta)$ spectrum and its use as a test of the overall performance of the detector. Appendix B discusses the extent to which the average value of the electron recoil energy is a good estimator of possible deviations from the CC shape expected in the absence of flavor violations.

II. NEUTRINO-RELATED INGREDIENTS

In this Section, we discuss the neutrino-related ingredients of the analysis that have appreciable, recognized uncertainties. These ingredients are: the ^8B neutrino spectrum (Sec. II A), the charged-current absorption cross section (Sec. II B), and the neutral-current dissociation cross section (Sec. II C). We discuss the detector-related ingredients in the following section.

A. ^8B neutrino spectrum

The only component of the solar neutrino spectrum [17] that is important for the SNO experiment is the ^8B spectrum, $\lambda(E_\nu)$. A derivation of the best-estimate ^8B spectrum, $\lambda(E_\nu)$, along with the maximum allowed deviations, $\lambda^\pm(E_\nu)$ (± 3 effective standard deviations away from the best-estimated spectrum) is presented in reference [6].

The ${}^8\text{B}$ neutrinos are produced in the decay ${}^8\text{B}(\beta){}^8\text{Be}$ followed by ${}^8\text{Be}(2\alpha)$ disintegration. The broad ${}^8\text{Be}$ intermediate state is responsible for important deviations of the neutrino spectrum λ from the usual allowed shape. The population of the ${}^8\text{Be}$ state is determined experimentally by measuring the delayed α -decay spectrum. The absolute energy calibration of the measured alpha spectrum is the main systematic error.

For the calculation of the ${}^8\text{B}$ neutrino spectrum, the experimental and theoretical uncertainties can be included [6] in a single effective alpha-energy offset, b : $E_\alpha \rightarrow E_\alpha + b$. The independently-measured positron spectrum in ${}^8\text{B}(\beta)$ decay [22] provides a fundamental additional constraint that was used in [6] to choose a “best” reference α -spectrum [23] and to bound its offset: $b = 0.025 \pm 0.104$ MeV ($\pm 3\sigma$ uncertainties). An “infinitely-precise” measurement of the ${}^8\text{B}(\beta)$ positron spectrum could reduce the effective $\pm 3\sigma$ range of b to ± 0.075 MeV, where 0.075 MeV is the residual theoretical uncertainty. The uncertainties of the ${}^8\text{B}$ neutrino spectrum would be reduced in the same ratio. Since the uncertainties in the neutrino spectrum are a significant source of errors for the CC-shape test with SNO, a reduction of the allowed range of b through more precise measurements of the ${}^8\text{B}$ positron spectrum would be useful.

The *hep* neutrinos [17] have a maximum energy of 18.8 MeV and could also in principle contribute to the neutrino spectrum observed by SNO. The calculated total flux of *hep* neutrinos is uncertain by a factor of about six [24] because of theoretical difficulties in estimating the low-energy production cross section. Using the nominal value $\phi_{\text{hep}} = 1 \times 10^{+3} \text{ cm}^{-2}\text{s}^{-1}$ given in [25], we estimate that *hep* neutrinos contribute less than 0.07% of either the total NC or CC event rates. Therefore, *hep* neutrinos can be neglected in calculating the CC/NC ratio. Moreover, we have verified that the *hep* contribution to the high-energy tail of the spectrum is much smaller than the shape uncertainties estimated below in Sec. IV A.

B. Charged current νd cross section

The cross section for the charged-current reaction (1) has been calculated a number of times in the last 30 years, since the original proposal by Jenkins [26] to use charged-current capture on deuterium to measure the ${}^8\text{B}$ solar neutrino flux. Kubodera and Nozawa [27] have recently presented an insightful and thorough summary of the calculations of both the charged current and the neutral current cross sections. In this subsection, we assess the reliability of the theoretical calculations of the total and the differential CC cross section. We establish the robustness of the calculated cross sections, which is exemplified by the excellent agreement between the simple effective range calculations and the more sophisticated treatments. In addition, we stress the importance for determining the shape of the electron spectrum of including the final state interactions among the protons. We discuss the neutral current cross section in the following subsection.

The kinematics of reaction (1) leads to the following expression [28] for the neutrino energy, E_ν :

$$E_\nu = Q + T_e + \frac{P^2}{m_p} + \frac{(\mathbf{p}_e - \mathbf{p}_\nu)^2}{4m_p} \quad , \quad (3)$$

where \mathbf{p}_ν is the neutrino 3-momentum, T_e and \mathbf{p}_e are the electron kinetic energy and 3-momentum, P is the relative momentum of the protons in the proton center-of-mass (c.m.s.) system, and the threshold $Q = 1.442$ MeV. The third term describes the kinetic energies of the two protons in the proton c.m.s. and is an important contribution to the energy balance. The fourth (last) term in Eq. (3) describes the small recoil energy of the two-proton center-of-mass system.

The charged-current absorption, reaction (1), is described by the well-known electroweak Hamiltonian and by less well-known nuclear physics effects that can be treated at various levels of approximation. A neutrino energy of 10 MeV corresponds in natural units to $(20 \text{ fm})^{-1}$. Therefore, we expect that the details of deuteron nuclear physics will play only a minor role. This expectation is confirmed by comparing the s -wave calculations performed in the 1960's by Kelly and Überall [29] and by Ellis and Bahcall [30] using Bethe's effective range approximation [31] with the recent sophisticated calculations by Ying, Haxton, and Henley [32] and by Kubodera and collaborators [33,27]. The recent calculations include higher partial waves, relativistic effects, forbidden matrix elements, and exchange-currents.

Figure 1a shows the excellent agreement between the effective-range calculations and the more sophisticated treatments. In the figure, three independent estimates of the total CC cross section are compared: Ellis-Bahcall (EB) [30], Kubodera-Nozawa (KN) [27], and Ying-Haxton-Henley (YHH) [32]. The main difference between the calculated cross sections of KN and YHH is an energy-independent normalization factor (about $\sim 6\%$ uncertainty, as also estimated in [27]). The EB normalization shows a slight energy dependence, that amounts to a $\sim 4\%$ additional variation over the important energy range of 5 MeV to 10 MeV. Figure 1b (referring to the neutral current cross-section) will be discussed in Sec. II C.

When quoting the Ellis-Bahcall cross-section [30], we use a slightly-improved calculation of the differential CC cross section in which we include the previously neglected p - p c.m.s. recoil term [the fourth term in Eq. (3)]. We have also used the more recent choices of parameters of the effective range approximation given in reference [34], in order to obtain our best estimate of the differential cross section $d\sigma_{CC}(E_\nu, T_e, \cos \theta)/dT_e d \cos \theta$ for any given value of E_ν , T_e and of the electron scattering angle θ .

Figure 2 shows the results of the improved Ellis-Bahcall calculation of the normalized differential cross section $\sigma_{CC}^{-1} d\sigma_{CC}/dT_e d \cos \theta$ (dotted line) as a function of the dimensionless variable $T_e/(E_\nu - Q)$, for representative values of E_ν and θ . The Kubodera-Nozawa results appear as a solid line in the same figure.³

The close agreement between the EB and KN normalized recoil electron spectra is striking. The angular dependence calculated using the effective range and the Hamiltonian approximations is essentially identical. On the basis of Fig. 2, we conclude that the uncertainties associated with the (T_e, θ) -shape of the normalized differential cross-section for the reaction (1) are much smaller than other recognized uncertainties. In practice, we parametrize the reference cross sections EB, KN, and YHH in the form:

³ The extensive numerical tables of the differential charged current cross section calculated by Kubodera and Nozawa in [27] are not published. We thank the SNO collaboration for providing us with a computer-readable copy of these tables.

$$\left[\frac{d\sigma_{\text{CC}}(E_\nu, T_e, \cos \theta)}{dT_e d \cos \theta} \right]_{\text{X}} = \sigma_{\text{CC}}^{\text{X}}(E_\nu) \left[\frac{1}{\sigma_{\text{CC}}(E_\nu)} \frac{d\sigma_{\text{CC}}(E_\nu, T_e, \cos \theta)}{dT_e d \cos \theta} \right]_{\text{EB}}, \quad (4)$$

for $\text{X} = \text{KN}, \text{YHH}$. The differences between the EB, KN and YHH cross sections are embedded in a multiplicative factor that depends exclusively on E_ν and not on the angular distribution.

Contrary to what is sometimes assumed in the literature (see, e.g., [19,35]), the electron spectra in Fig. 2, although peaked, cannot be approximated well by delta functions in the electron energy. In other words, there is not a one-to-one relation between the incoming neutrino's energy and the energy of the electron that is produced. The final state in the charged current reaction cannot be approximated by a pure two-body state. Even as early as the seminal Kelly-Überall calculation [29], it was noted that the attractive 1S p - p interaction is not sufficient to bind the protons as an effective single particle, because of the presence of the repulsive Coulomb force. The two-body approximation would be equivalent to omitting the third and fourth terms in Eq. (3). Removing only the fourth (the smallest) recoil term in Eq. (3) would cause the dotted cross sections in Fig. 2 to be systematically peaked at slightly higher electron energies (about +2% at $E_\nu = 12$ MeV). The excellent agreement between our improved Ellis-Bahcall calculation and the Kubodera-Nozawa differential cross sections would be spoiled by omitting even this smallest term.

C. Neutral current νd cross section

We use the recent calculations of the neutral current cross sections (averaged over final states), $\sigma_{\text{NC}}(E_\nu)$, by Kubodera and Nozawa (KN) [27], and by Ying, Haxton and Henley (YHH) [32]. Only the total rate for reaction (2), not the differential production rate as a function of energy, will be measured by SNO. However, the energy dependence of the cross section for the neutral current reaction is relevant for the SNO experiment, since the calculated differential cross section will be used in the SNO Monte Carlo simulations to model the production, and subsequent detection, of the neutrons produced by the neutral current reaction.

Figure 1b compares the KN and YHH neutral current cross section as a function of neutrino energy. The difference is $\sim 6\%$, about the same magnitude and in the same direction as for the charged current cross section. There is a small residual energy-dependence below $E_\nu \simeq 6$ MeV. The difference shown in Figure 1b between the theoretical calculations is consistent with the theoretical error of $\pm 10\%$ that was estimated by Bahcall, Kubodera, and Nozawa [36] from various contributions (the impulse approximation, the nucleon-nucleon potential, meson exchange currents, and higher partial waves).

The best estimate (and 1σ uncertainty) for the neutral current cross section averaged over the ^8B neutrino spectrum is

$$\langle \sigma(^8\text{B}) \rangle = 0.478(1 \pm 0.06) \times 10^{-42} \text{ cm}^2. \quad (5)$$

We have chosen in Eq. (5) the 1σ error of 6% to reflect the difference between the KN and YHH calculations. The standard solar model [25] prediction for the neutral current event rate due to ^8B neutrinos is

$$\langle\phi\sigma\rangle = 3.2_{-0.5}^{+0.6} \text{ SNU}, \quad (6)$$

where the quoted 1σ error in Eq. (6) combines quadratically the uncertainties in the solar model prediction, the ^8B neutrino spectrum, and the neutral current cross section. The uncertainties in the solar model calculation dominate the error estimate. The event rate SNU is defined [37] as 10^{-36} interactions per target atom (deuterium atom) per second.

In the calculation of the CC/NC rate, the (already-small) theoretical cross section errors largely cancel and therefore do not affect significantly the ratio. As a default choice, we use the KN neutral current cross section in our calculations. The YHH cross section is used for comparison and to evaluate the theoretical uncertainties.

III. DETECTOR-RELATED INGREDIENTS

In this section, we discuss the detector-related ingredients of the analysis: the energy resolution, the absolute energy scale, the detector efficiencies, and the energy threshold for detecting CC events. Accurate determinations of all of these experimental quantities, and their associated uncertainties, are significant for the success of the SNO experiment.

A. Energy Resolution

The measured electron kinetic energy, T_e , determined by SNO with the Cherenkov technique, will be distributed around the *true* energy T'_e with a width established by the photon statistics.

The resolution function $R(T'_e, T_e)$ is expected to be well approximated by a normalized Gaussian,

$$R(T'_e, T_e) = \frac{1}{\sigma(T'_e)\sqrt{2\pi}} \exp\left[-\frac{(T'_e - T_e)^2}{2\sigma(T'_e)^2}\right] \quad (7)$$

with an energy-dependent one-sigma width $\sigma(T'_e)$ given by [17,38]

$$\sigma(T'_e) = \sigma_{10}\sqrt{\frac{T'_e}{10 \text{ MeV}}}, \quad (8)$$

where σ_{10} is the resolution width at $T'_e = 10 \text{ MeV}$. A plausible estimate of the parameter σ_{10} is 1.1 MeV ($\sigma_{10} = 1.8 \text{ MeV}$ for Kamiokande, see [38]), and σ_{10} itself may be uncertain by 10% [39]. We will use in what follows $\sigma_{10} = 1.1 \pm 0.11 \text{ MeV}$ (1σ errors) as an illustrative estimate.

In Figure 3, solid line, we anticipate the results of our best-estimate of the standard shape of the electron energy spectrum (see Sec. IV). The dotted line in Fig. 3 represents the same spectrum without the inclusion of the energy resolution. The area under the curve is normalized to unity in both cases.

B. The Absolute Energy Scale

What is the absolute accuracy of the SNO energy scale? How precisely will the average SNO energy measurement correspond to the true electron energy?

The energy resolution function of the previous section describes how the measured kinetic energy, T_e , is distributed around the true energy, T'_e , assuming that the centroid of the distribution, $T_{e,\text{ave}}$, coincides with T'_e . The calibration of the energy scale will be performed with a series of γ -ray sources, the most important of which are monoenergetic. The primary energy calibration source will be the 6.130 MeV γ -ray from the decay of the first 3^- excited state in ^{16}O . We define the systematic error in the absolute energy calibration, δ , by the relation

$$\delta \equiv T_{e,\text{ave}} - T'_e . \quad (9)$$

A reasonable 1σ estimate [39] of δ is:

$$\delta = \pm 100 \text{ keV} \left(\frac{T'_e}{10 \text{ MeV}} \right)^\alpha , \quad 0 \leq \alpha \leq 1 , \quad (10)$$

which corresponds to a $\pm 1\%$ error at 10 MeV. For comparison, the Kamiokande collaboration achieved [38] a $\pm 3\%$ energy scale error.

The case $\alpha = 0$ ($\alpha = 1$) would correspond to an energy-independent scale shift (scale factor). The intermediate case $\alpha = \frac{1}{2}$ would apply to a scale uncertainty dominated by the width of calibration lines (error $\propto \sqrt{T'_e}$).

In general, the phenomenological parameter α will depend both on the physical sources of the scale uncertainties and on the calibration technique. It may even remain an unknown parameter after calibration. However, as we will see, the energy-scale induced uncertainties of the SNO observables depend only mildly on α . The worst case appears to be $\alpha = 0$ (i.e., a uniform energy bias), which we adopt for a conservative estimate of the errors.

In practice, we introduce the energy scale shift δ by modifying the energy resolution function [Eq. (7)] with the replacement:

$$R(T'_e, T_e) \longrightarrow R(T'_e + \delta, T_e) \quad (11)$$

and δ given by Eq. (10). The reader can verify that the transformation given in Eq. (11) is an appropriate representation of the energy-calibration uncertainty by writing the total rate for the process under consideration as a triple integral over the neutrino energy (E_ν), the true electron recoil energy (T'_e), and the measured electron recoil energy (T_e , between a specified minimum and maximum value).

C. Detection efficiencies

The detection efficiencies, ϵ_{CC} and ϵ_{NC} , for detecting charged and neutral current events, will be measured with calibration experiments at SNO along with their uncertainties, $\sigma(\epsilon_{\text{CC}})$ and $\sigma(\epsilon_{\text{NC}})$. The calibration experiments will also measure possible variations of the CC

efficiency with the (true) electron recoil energy, $\epsilon_{CC} = \epsilon_{CC}(T'_e)$, which can in principle affect the CC-shape measurements. If the experiments work as expected [40], then $\sigma(\epsilon_{CC}) < \sigma(\epsilon_{NC})$ and

$$\sigma(\epsilon_{NC}) \simeq 2\% \quad (1\sigma) \quad . \quad (12)$$

In Sec. IV, we shall include the efficiencies $\epsilon_{CC}(T'_e)$ and ϵ_{NC} in the general expressions for the predicted quantities. As default values, we will assume that $\epsilon_{CC}(T_e)$ is constant and equal to 1, and that $\epsilon_{NC} = 0.50 \pm 0.01$ (1σ error). It will be shown in Sec. IV C that plausible energy variations of ϵ_{CC} induce deviations in the CC spectrum that are much smaller than other sources of error.

In any event, after $\epsilon_{CC}(T'_e)$ and ϵ_{NC} are measured in the SNO detector, their effects on the predictions, and their uncertainties, can be included easily using the formalism given here.

D. Threshold Energy

The measured kinetic energy threshold, T_{\min} , for counting charged current events is expected to be fixed around 5 MeV [1]. Below ~ 5 MeV, the signal-to-background ratio is expected to decrease very rapidly. In principle, one would like to have the threshold as low as possible in order to increase the number of events that are detected for a given exposure and in order to observe more of the curvature of the spectrum at lower energies (cf. Fig. 3). The actual background level in the operating SNO detector will determine how low the energy threshold may be set. In Sec. V C, we will show that the discriminatory power of the experiment is not very sensitive to the actual threshold level as long as the threshold is in the vicinity (± 1 MeV) of the nominal value, $T_{\min} = 5$ MeV.

IV. STANDARD NEUTRINO PHYSICS AT SNO

In this section, we calculate the standard predictions, and their associated uncertainties, for the shape of the CC electron recoil energy spectrum and the ratio of total number of CC to NC events. We assume standard neutrino properties (lepton flavor conservation and zero neutrino masses) and the ingredients discussed in the previous sections (Secs. II and III). We adopt the Kubodera-Nozawa (KN) neutrino interaction cross sections as “standard,” since they are the most recent and complete for both the charged and the neutral current reactions. In particular, we evaluate the standard CC differential cross-section as indicated by Eq. (4) with $X = \text{KN}$, i.e., with absolute normalizations given by the Kubodera-Nozawa [27] calculations and relative differential cross sections given by the Ellis-Bahcall [30] calculation.

The shape of the recoil electron energy spectrum is given by the normalized distribution of charged current events (N_{CC}) as a function of the measured kinetic energy, T_e :

$$\frac{1}{N_{CC}} \frac{dN_{CC}}{dT_e} = \frac{\int dE_\nu \lambda(E_\nu) \int dT'_e \frac{d\sigma_{CC}}{dT'_e} R(T'_e, T_e) \epsilon_{CC}(T'_e)}{\int_{T_{\min}} dT_e \int dE_\nu \lambda(E_\nu) \int dT'_e \frac{d\sigma_{CC}}{dT'_e} R(T'_e, T_e) \epsilon_{CC}(T'_e)} \quad , \quad (13)$$

where T_{\min} is threshold for the measured electron kinetic energy and $\epsilon_{\text{CC}}(T'_e)$ is the efficiency for detecting an electron of true energy T'_e . The energy resolution function, $R(T'_e, T_e)$, is given by Eq. (7), with an allowance for an energy scale shift [Eqs. (10, 11)]. The CC differential cross section, $\frac{d\sigma_{\text{CC}}}{dT'_e}$, is implicitly integrated over the entire solid angle since events will be detected for all electron recoil angles.

The ratio of charged to neutral current events may be written:

$$\frac{N_{\text{CC}}}{N_{\text{NC}}} = \frac{\int_{T_{\min}} dT_e \int dE_\nu \lambda(E_\nu) \int dT'_e \frac{d\sigma_{\text{CC}}}{dT'_e} R(T'_e, T_e) \epsilon_{\text{CC}}(T'_e)}{\epsilon_{\text{NC}} \int dE_\nu \lambda(E_\nu) \sigma_{\text{NC}}(E_\nu)}, \quad (14)$$

where ϵ_{NC} is the overall efficiency of neutral current event detection.

It is necessary to adopt specific values for the efficiencies ϵ_{CC} and ϵ_{NC} in order to evaluate the relative *number* of CC and NC events and thus the statistical errors. We adopt plausible default values, $\epsilon_{\text{CC}} = 1$ and $\epsilon_{\text{NC}} = 0.50$. However, after calculating the statistical and efficiency errors, we prefer to convert the results to, and to quote, an essentially efficiency-independent CC/NC ratio, $R_{\text{CC}}/R_{\text{NC}}$, defined as

$$\frac{R_{\text{CC}}}{R_{\text{NC}}} = \frac{\epsilon_{\text{NC}} N_{\text{CC}}}{\epsilon_{\text{CC}} N_{\text{NC}}}. \quad (15)$$

In writing Eq. (15), we have assumed that ϵ_{CC} is equal to a constant, which turns out to be a good approximation.

A. Standard model predictions for the CC spectrum shape

What effects do the different uncertainties have on the shape of the electron energy spectrum? Figure 4 answers this question by showing the standard spectrum (solid line) and the effective 3σ shape errors (dashed lines) due to neutrino-related and to detector-related uncertainties. We postpone the discussion of the sensitivity of the results to the assumed CC threshold energy to Section V C (see especially Tables III and IV).

The dominant neutrino-related uncertainties are due to the ${}^8\text{B}$ neutrino energy spectrum $\lambda(E_\nu)$ (Fig. 4a). The theoretical CC cross section uncertainties are very small; Fig 4b shows the “greatest” deviation, induced by the use of the EB instead of the KN cross-sections.

The detector related uncertainties are due to statistics (Fig. 4c), energy resolution (Fig. 4d), and energy scale (Figs. 4e,f). The statistical errors bars in Fig. 4c refer to a hypothetical sample of 5000 CC events collected above threshold and divided in 10 bins. In Fig. 4d, the dotted curves have been obtained by using energy resolution widths $\sigma_{10} = 1.1 \pm 0.33$ MeV ($\pm 3\sigma$ errors, see Sec. III A). The last two subplots of Fig. 4 show the effect of the absolute scale uncertainty, with $\alpha = 0$ or $\alpha = 1$ (see Sec. III B). The two cases are almost indistinguishable. We adopt in the following the value $\alpha = 0$, since it gives slightly more conservative error estimates.

Figure 4 shows that the systematic errors due to the adopted uncertainties in the energy scale, in the resolution width and in the ${}^8\text{B}$ neutrino spectrum are at least as important as the statistical errors, with the additional complication that the non-statistical errors are

correlated point-by-point. The correlations of the uncertainties imply that the analysis of a realistic spectrum divided in N bins could become rather cumbersome, requiring consideration of an $N \times N$ covariance matrix with large off-diagonal elements for the usual χ^2 statistics. Moreover, the χ^2 test is not powerful when bins are affected by significant systematic errors, since the additional information embedded in sequences of equal-sign deviations (typically all positive or all negative in one half of the spectrum, as in Fig. 4) is lost.

The simplest quantity that characterizes a generic electron spectrum, while avoiding the use of bins, is the average value of the measured recoil energy, $\langle T_e \rangle$ (see also [19,20]).⁴ The basic question then becomes: “Can SNO detect significant deviations of $\langle T_e \rangle_{\text{measured}}$ from $\langle T_e \rangle_{\text{standard}}$?”

We evaluate $\langle T_e \rangle$ with the aid of Eq. (13) by using the definition

$$\langle T_e \rangle \equiv \int_{T_{\min}} dT_e T_e \frac{1}{N_{\text{CC}}} \frac{dN_{\text{CC}}}{dT_e} . \quad (16)$$

We determine the effects of uncertainties in different ingredients by carrying out the integration indicated in Eq. (16) with different assumptions. For example, we estimate the 1σ uncertainty associated with the neutrino spectrum by evaluating $\langle T_e \rangle$ using the neutrino spectra $\lambda^+(E_\nu)$, $\lambda^-(E_\nu)$, which are $\pm 3\sigma$ away from the best-estimate neutrino spectrum [6]. Then the 1σ difference is $\sigma(\langle T_e \rangle) = \frac{1}{6}[\langle T_e(\lambda^+) \rangle - \langle T_e(\lambda^-) \rangle]$. Analogously, the 1σ errors due to the energy resolution uncertainties were estimated by recalculating the spectra, and thus $\langle T_e \rangle$, with $\sigma_{10} = 1.1 \pm 0.33$ MeV ($\pm 3\sigma$), and dividing the total shift by six. A similar procedure was adopted for determining the energy scale error. For the CC cross section uncertainty, we have attached a 1σ significance to the deviation obtained when the Ellis-Bahcall CC cross sections were used instead of the Kubodera-Nozawa CC cross sections, i.e., $\sigma(\langle T_e \rangle) = \langle T_e(\text{EB}) \rangle - \langle T_e(\text{KN}) \rangle$.

Our standard estimate, for $T_{\min} = 5$ MeV, is then:

$$\begin{aligned} \langle T_e \rangle &= 7.658 \pm 0.025^a \pm 0.011^b \pm 0.029^c \pm 0.024^d \pm 0.052^e \text{ MeV} , \\ &= 7.658 \cdot (1 \pm 0.009) \text{ MeV} , \end{aligned} \quad (17)$$

where the errors ($\pm 1\sigma$) are due to: a) statistics of 5000 CC events; b) difference between EB and KN cross sections; c) uncertainties in the neutrino spectrum; d) energy resolution; and e) the absolute energy calibration. The statistical error of the average is calculated, according to the central limit theorem, as $\sigma_{\text{stat}} = \sqrt{\text{Var}/N_{\text{CC}}}$, where Var is the variance of the standard distribution above threshold, $\text{Var} = (1.74 \text{ MeV})^2$.

The assumed uncertainty in the absolute energy scale, Eq. (10), dominates the total error.

In the best-estimate calculation, the detection efficiency ϵ_{CC} has been taken constant. A linear dependence of ϵ_{CC} on T_e (neglecting temporarily the distinction between measured and true energies, T_e and T'_e) would modify the CC spectrum as:

⁴For a discussion of the extent to which the average electron recoil energy is a good estimator of the deviations from the expected shape in the absence of electron flavor violation, see Appendix B and Ref. [41].

$$\frac{1}{N_{\text{CC}}} \frac{dN_{\text{CC}}}{dT_e} \longrightarrow \frac{1}{N_{\text{CC}}} \frac{dN_{\text{CC}}}{dT_e} \left(1 + \beta \frac{T_e - \langle T_e \rangle}{\langle T_e \rangle} \right) \quad (18)$$

and the average value as

$$\langle T_e \rangle \longrightarrow \langle T_e \rangle \left(1 + \beta \frac{\text{Var}}{\langle T_e \rangle^2} \right) \quad (19)$$

where β is the slope of $\epsilon_{\text{CC}} = \epsilon_{\text{CC}}(T_e)$. A plausible variation (or uncertainty) of ϵ_{CC} over the interval 5–15 MeV is a few percent, say 3% for definiteness. This would correspond to $\beta = 0.023$ and to a 0.12% variation of $\langle T_e \rangle$, comparable to the smallest error shown in Eq. (17). We conclude that uncertainties in the CC efficiency will not be an important source of error, if SNO performs as expected.

The characterization, Eq. (16), of the spectrum given in Eq. (13) is the first (non-trivial) step in a complete description by a series of moments: the zeroth moment (the area), the first moment (the average), the second moment (the variance), and higher-order moments. In the present case, the zeroth moment is equal to unity by definition, and small variations in the shape of the spectrum affect primarily the average value. More sophisticated unbinned tests, such as the Kolmogorov-Smirnov (K-S) test, may be useful to apply after the SNO collaboration has estimated by empirical calibrations the systematic errors in the experimental input quantities. One could then determine by Monte Carlo simulations the distribution function for the K-S statistic with an inferred model for the systematic errors.

B. Standard model predictions for the CC/NC ratio

In Eq. (15), we have defined a charged to neutral current ratio, $R_{\text{CC}}/R_{\text{NC}}$, which is independent of the average absolute values of the efficiencies but incorporates the efficiency-induced errors.

The calculation of the standard value and $\pm 1\sigma$ errors for $R_{\text{CC}}/R_{\text{NC}}$ is done with the same logic as for $\langle T_e \rangle$. The final result is:

$$\begin{aligned} \frac{R_{\text{CC}}}{R_{\text{NC}}} &= 1.882 \pm 0.058^a \pm 0.010^b \pm 0.008^c \pm 0.009^d \pm 0.034^e \pm 0.038^f \\ &= 1.882(1 \pm 0.042) \quad . \end{aligned} \quad (20)$$

The individual contributions result from: a) statistics of 5000 CC events and 1354 NC events ($\epsilon_{\text{NC}} = 0.5$); b) difference between YHH and KN cross sections; c) neutrino spectrum; d) energy resolution; e) energy scale; f) NC efficiency.

C. Correlation of errors

Some of the systematic errors affecting $\langle T_e \rangle$ and $R_{\text{CC}}/R_{\text{NC}}$ have the same origin and are correlated. In particular, a variation of the neutrino spectrum $\lambda(E_\nu)$ causes both $\langle T_e \rangle$ and $R_{\text{CC}}/R_{\text{NC}}$ to increase or decrease at the same time. A variation of σ_{10} , the energy resolution

width, produces instead opposite effects (anti-correlation). Energy scale errors are positively correlated.

In Table I, we summarize the separate error components and their correlations. The correlation of the total errors, $\rho = 0.32$, is small because of accidental cancellations, but it is not entirely negligible. When the actual error budget for SNO is determined experimentally, the approximate cancellation of the correlations may not be as strong.

V. COULD SNO PROVE THE OCCURRENCE OF NEW PHYSICS?

In the previous section, we calculated the standard predictions for the CC-shape and the CC/NC ratio, $\langle T_e \rangle$ and R_{CC}/R_{NC} , along with a realistic estimate of these uncertainties. In this section, we show that the anticipated uncertainties are sufficiently small to allow SNO to prove the occurrence of new physics with a high degree of confidence.

A. Neutrino oscillations

We examine the implications of three representative scenarios in which the solar neutrino problem is solved by neutrino oscillations: the two (best-fit) Mikheyev-Smirnov-Wolfenstein (MSW) [42] solutions at small and at large mixing angle (SMA and LMA), and the purely vacuum (VAC) oscillation [43] solution (see [44] and refs. therein).⁵

Figure 5 illustrates some of the principal differences among the three oscillation scenarios and also shows that all of the oscillation solutions differ significantly from the standard model expectations (STD). The survival probabilities for electron-type neutrinos vary greatly among the oscillation scenarios, as can be seen clearly in Fig. 5a. The energy spectrum of electron-type neutrinos at earth, shown in Fig. 5b, is affected strongly by oscillations. Figure 5c represents the different CC electron recoil spectra that are predicted for SNO, with the normalization: Area = 1. Until the neutral current is measured, the different recoil spectra must be compared with the same normalization, as in Fig. 5c, because we do not know *a priori* the total number of electron-type neutrinos that are created in the solar interior. Once the neutral current is measured, we can compare the different oscillation and no-oscillation scenarios in a more informative way. Figure 5d makes use of assumed measurements of the total neutral and charged current rates and shows the standard electron spectra normalized to Area = N_{CC}/N_{NC} .⁶ A comparison of Figs. 5c and Fig. 5d makes clear

⁵The best-fit mass and mixing values (Δm^2 , $\sin^2 2\theta$) are taken from [44]: (5.4×10^{-6} eV², 7.9×10^{-3}) for small angle MSW, (1.7×10^{-5} eV², 0.69) for large angle MSW, and (6.0×10^{-11} eV², 0.96) for vacuum oscillations. Numerical tables of the oscillation probabilities for these best-fit scenarios were prepared by P. Krastev [44] and are available at the following URL: <http://www.sns.ias.edu/~jnb>.

⁶If we had normalized the area to the efficiency-independent ratio, Area = R_{CC}/R_{NC} , then the scale of the ordinate in Fig. 5d would be decreased by a factor of 2, but the relative shapes would

the importance of the neutral current measurement for interpreting the shape of the electron recoil spectrum.

Figure 6 shows the ratio of the normalized electron spectra after oscillation (as displayed in Fig. 5c) to the standard spectrum. These ratios of spectra are approximately linear in energy. Therefore, the main effect of oscillations on the normalized CC spectrum is to change the first moment of the energy distribution, i.e., the mean value $\langle T_e \rangle$. In Ref. [20], it is shown that the approximate linearity of the ratios of recoil energy spectra is a general feature of the resonant MSW effect. The representation of the spectral information by one parameter, $\langle T_e \rangle$, is efficient because the ratios of spectral shapes are approximately linear (i.e., are determined rather well by just one parameter).

B. Statistical analysis

For the three neutrino oscillation scenarios considered in the previous section, we calculate the observables $\langle T_e \rangle$, R_{CC}/R_{NC} , and their distance—in units of standard deviations—from the standard predictions, Eqs. (17) and (18).

For each test, the distance is defined simply as:

$$\mathcal{N}(\sigma) = (X - X_{\text{standard}})/\sigma_{X,\text{standard}} \quad , \quad (21)$$

where $X = \langle T_e \rangle$, R_{CC}/R_{NC} . In the combined tests, we have calculated the χ^2 including the correlation of the total errors (see Table I), and defined $\mathcal{N}(\sigma) = \sqrt{\chi^2}$ [3]. When $\mathcal{N}(\sigma) \gg 3$, the physical interpretation is that the statistical probability of the result under consideration is negligibly small; the normal distribution presumably does not describe the extreme tails of the probability distribution.

The expected deviations for different oscillation scenarios are shown in Table II.

The measurement of the R_{CC}/R_{NC} ratios is a powerful test for occurrence of new physics; the three oscillation cases are each separated from the standard expectations by a distance that is formally more than 15σ (cf. comment above regarding $\mathcal{N}(\sigma) \gg 3$).

The CC-shape test is less powerful. This is of course expected for the large-angle MSW case, but is somewhat surprising for the small-angle MSW case, that was generally expected to be separated from the standard model expectations at a high confidence level [19,20]. The reason that the significance level found here for the measurement of the CC shape is much less than previously calculated is that we have included estimates for the systematic uncertainties. The systematic errors in measuring the CC-shape may be twice as large as typical statistical errors (5000 CC events in our case), as evidenced in Table I. The statistical power of the combined tests (CC-shape and NC/CC) is dominated by the measurement of the CC/NC ratio. The effect of the correlation of the errors is small but not entirely negligible.

Figures 7 and 8 display graphically the information contained in Tables I and II. In Fig. 7 we show the standard predictions for $\langle T_e \rangle$ (upper panel) and R_{CC}/R_{NC} (lower panel), together with the separate and combined 3σ errors. The values of $\langle T_e \rangle$ and R_{CC}/R_{NC} for

remain the same.

the different oscillation channels are also displayed. In Fig. 7a, the efficiency error (labeled by a question mark) should be negligible if SNO works as expected.

In Fig. 8 we show the results of the combined tests (correlations included) in terms of iso-sigma contours in the plane $(\langle T_e \rangle, R_{CC}/R_{NC})$, where $\mathcal{N}(\sigma) = \sqrt{\chi^2}$. The three oscillation scenarios can be well separated from the standard case, but the vertical separation (R_{CC}/R_{NC}) is larger and dominating with respect to the horizontal separation ($\langle T_e \rangle$).

The error bars on the SMA point in Fig. 7 and Fig. 8 represent the range of values allowed at 95% C.L. by a fit of the oscillation predictions to the four operating solar neutrino experiments [44]; they are intended to indicate the effect of the likely range of the allowed oscillation parameters.

The choice of $\langle T_e \rangle$ as a characterization of the CC-shape is not unique. $\langle T_e \rangle$ has been chosen because it is a single and well-defined number (the first moment of the electron distribution), whose systematic uncertainties can be determined independent of the event binning. If the measured electron distribution at SNO has significant deviations of the second moment (the variance), or higher moments, from the standard expectations, then $\langle T_e \rangle$ may not be the optimal statistical estimator. If a more sophisticated statistical test is used to test for non-standard curvature in the spectrum, then the assessment of statistical significance will require a full Monte Carlo simulation of SNO detector, with systematic effects calculated by brute force.

C. Threshold Dependences

All of the previous calculations were carried out assuming an recoil energy threshold, T_{\min} , of 5 MeV. The actual value of T_{\min} that will be used will depend upon the observed or estimated backgrounds in the operating SNO detector.

Table III summarizes the dependence of $\langle T_e \rangle$ and R_{CC}/R_{NC} on the adopted energy threshold. We give values for the standard model and for the three exemplary oscillation scenarios.

In Table IV we give the distances of the oscillation scenarios from the standard predictions, in units of standard deviations.

We see from Tables III and IV that the differences resulting from changing the threshold by ± 1 MeV are not expected to be decisive for the SNO discovery potential. However, the diagnostic power of the measurement of the shape of the electron recoil energy spectrum would be significantly enhanced if the energy threshold were lowered. The small mixing angle MSW solution is 3.8σ away from the standard model prediction if the threshold is 4 MeV but is only 2.4σ away if the threshold is 6 MeV.

VI. SUMMARY AND CONCLUSIONS

The Sudbury Neutrino Observatory has the potential to reveal new phenomena with a high level of confidence, but the detector must work well in order to discriminate among different physics options. The accurate calibration of the absolute energy scale, the energy resolution width for electron detection, and a high sensitivity for neutral current detection, are especially important.

We have determined both the the best-available estimates and the uncertainties of three important neutrino-related input quantities (available at the following URL: <http://www.sns.ias.edu/~jnb>) that will be needed in the analysis of the SNO data: the laboratory shape of the ^8B neutrino energy spectrum, the charged current neutrino absorption cross section, and the neutral current dissociation cross section.

We have also estimated the effects on the tests of electron flavor violation of five detector-related aspects: the energy resolution, the absolute energy scale, the energy threshold, and the detection efficiencies of the charged current events and of the neutral current events.

The principal uncertainties that affect the predictions are shown in Table I and in Fig 7. For the measurement of the shape of the electron recoil energy spectrum, the largest estimated error is contributed by the uncertainty in the absolute energy scale, with significant additional errors arising from the energy resolution and from the shape of the ^8B neutrino energy spectrum.

Unfortunately, the systematic uncertainties reduce the power of SNO to detect new physics via the measurement of the shape of the recoil electron spectrum. For example, a previous analysis [20], which considered only statistical errors, indicated that a 3σ distinction between the standard model prediction and the small angle MSW solution would be possible with only 1800 CC events observed with the SNO observatory. This same statistical-only analysis suggests that 5000 CC events would give more than an 8σ distinction. With our adopted estimates of the systematic uncertainties and 5000 CC events, we find that, instead of 8σ , the standard model prediction and the best-fit small angle MSW solution differ by only 3.1σ , as judged by $\langle T_e \rangle$. Even with zero statistical error, the difference between the standard model prediction and the small angle MSW solution would be only 3.3σ . Indeed, the systematic uncertainties begin to dominate the statistical uncertainties for this case after (less than) a year of operation. The statistical significance can be improved by $\sim 1\sigma$ for the SMA solution if the variance of the spectrum as well as $\langle T_e \rangle$ is measured [41]. Fortunately, the shape of the recoil spectrum predicted by vacuum neutrino oscillations is distinctive and the difference between standard model physics and vacuum oscillations represents, with our adopted uncertainties, a 10σ distinction in the SNO detector.

The main information content of the measured shape of the electron recoil spectrum can be summarized by evaluating the average recoil electron energy. For standard model physics, we find that the average electron kinetic energy is $\langle T_e \rangle = 7.658(1 \pm 0.009)$ MeV, 1σ total errors.

Figure 5c compares the normalized electron recoil spectra computed for the standard model, the LMA, the SMA, and the vacuum neutrino oscillation scenarios. The differences in the positions of the peaks of the spectra shown in Fig. 5c are larger than the differences in $\langle T_e \rangle$ given in Table II and Table III. Although previous authors have shown similar figures with error bars due only to the statistical fluctuations assigned to individual bins, we refrain from showing error bars in Fig. 5c since the systematic errors will likely dominate the statistical uncertainties and since systematic errors are correlated from bin to bin.

There is not a one-to-one relation between the incoming neutrino energy in the charged current reaction and the energy of the electron that is produced. Figure 2 shows, in fact, that there is a significant spread in electron recoil energies for a specified neutrino energy. This result, unfortunately, contradicts the assumption of a one-to-one energy relation used by a number of authors [19,35] in describing potential applications of SNO measurements.

The neutral current to charged current event ratio is a sensitive probe of lepton flavor violation. For standard model physics, we find a charged-to-neutral current ratio $R_{\text{CC}}/R_{\text{NC}} = 1.882(1 \pm 0.042)$, 1σ total error.

The measurement of the absolute neutral current rate will test directly the solar model prediction [25] of $3.2^{+0.6}_{-0.5}$ SNU, 1σ total error, for the ^8B neutrino flux. This test of solar models is independent of uncertainties in the fundamental physics related to oscillations into active neutrinos.

The predictions of the three favored oscillation solutions considered here (small mixing and large mixing MSW solutions, and vacuum oscillations) are all separated by more than 16σ from the predictions of the standard model with no lepton flavor violations, as shown in Table II and Fig. 8. The combined test, shape of the electron recoil spectrum and ratio of neutral current events to charged events, is, in our simulations, only slightly more powerful than the neutral current to charged current ratio alone.

An accurate measurement of the neutral current rate is essential in order to exploit the full potential for new physics of the Sudbury Neutrino Observatory.

Are the conclusions about the statistical significance of the flavor tests robust with respect to the SNO charged-current energy threshold? This question is answered in Table III and Table IV. These two tables show that the discriminatory ability of the SNO detector does not depend critically upon the detection threshold for the CC reaction. However, lowering the threshold to 4 MeV would separate by the shape measurement alone the small mixing angle MSW solution by 3.8σ from the standard prediction, instead of the 3.1σ that applies for a threshold of 5 MeV.

The relative insensitivity of the diagnostic power of SNO to the CC energy threshold suggests one possible strategy for dealing, especially in the initial stages of the experiment, with the most troubling backgrounds. Without seriously affecting the discriminatory power of the CC to NC ratio (see Table III and Table IV), the CC energy threshold for events being analyzed can be set sufficiently high, at 6 MeV or perhaps even at 7 MeV, that no significant background contamination is plausible.

Are the absolute event rates for the CC events sensitive to the assumed CC threshold? Table V gives the expected event rates for different assumed thresholds and neutrino oscillation scenarios. The range of expected event rates is about a factor of two for CC thresholds from 4 MeV to 7 MeV for the standard model and for the SMA and LMA MSW solutions; the variation is about 40% for the vacuum oscillations.

We have also varied the assumed value of the energy resolution width at 10 MeV, σ_{10} . We find that a one-third worsening of the energy resolution σ_{10} , which is defined by Eq. (8), from the current best-guess of 1.1 MeV to 1.5 MeV decreases the difference between the standard model value for $\langle T_e \rangle$ and the small mixing angle (MSW) value from 3.1σ to 2.8σ . Thus it is important that the energy resolution width is kept as low as possible.

The expected background level in SNO decreases strongly with increasing energy [1]. Increasing the electron energy threshold for the charged current reaction, can decrease the fractional contribution of background events.

The principal lesson of Table III and Table IV is that the SNO experiment will provide a powerful diagnostic for new physics even if the observed backgrounds are somewhat higher than expected.

We have varied the mass and mixing parameters of the small mixing angle (MSW) case

within the 95% C.L. limits of the fit to the four operating experiments [44]. The difference between the standard value of $\langle T_e \rangle$ and the value calculated for the small mixing angle solution varies between 3.1 ± 0.6 standard deviations, depending on which values one adopts within the allowed MSW region. (Somewhat more powerful discrimination can be achieved if both the dispersion and the mean recoil energy are calculated [41].) The formal difference between the standard and the MSW value of R_{CC}/R_{NC} is always within 15.7 ± 1.6 standard deviations at 95% C.L. Thus the MSW solution at small mixing angles (SMA) can be tested with a high level of confidence with the SNO experiment, although the information coming from the CC-shape might not be sufficient by itself.

We discuss in Appendix A the information that can be gained from an overall test of the SNO detector using an intense ${}^8\text{Li}(\beta^-)$ source. We calculate a theoretical ${}^8\text{Li}(\beta^-)$ spectrum and compare with the available data. We conclude that the existing data for the ${}^8\text{Li}(\beta^-)$ spectrum are not sufficient to permit an accurate test of the SNO detector and that a new, laboratory experiment is required.

Appendix B discusses the extent to which $\langle T_e \rangle$ is a good statistical estimator of possible deviations in the CC electron spectrum.

Finally, we must ask: How general are the conclusions given in this paper? The method of analysis and the discussion of the principal ingredients and their uncertainties will be of use in considering how well SNO can test potential new physics scenarios. We have evaluated the sensitivity of the likely operation of the Sudbury Neutrino Observatory to the MSW and vacuum neutrino oscillations that best-fit (see [44]) the results of the four pioneering solar neutrino experiments. The correct physical explanation may differ from the oscillation solutions considered here. The “true” solution of the solar neutrino problems may involve, for example, a distortion of the CC electron recoil spectrum that is much more drastic than is implied by the oscillation solutions considered here. In this case, the shape of the electron recoil spectrum from the CC reaction might indicate new physics that is not apparent by comparing the rates of the CC and the NC reactions [35]. The analysis presented in this paper is illustrative of the power of the SNO detector, but specific, quantitative inferences depend upon what, if any, new physics exists in the accessible domain.

ACKNOWLEDGMENTS

We are grateful to the SNO collaboration for providing information on the best-estimates and uncertainties for the experimental quantities. In addition, we are especially grateful to F. Ajzenberg-Selove, H. A. Bethe, F. Calaprice, W. C. Haxton, B. R. Holstein, E. Kolbe, P. I. Krastev, K. Kubodera, Y. Nir, W. Press, A. Yu. Smirnov, and J. Sromicki for valuable advice, discussions, and suggestions. For important comments on an early draft of this paper, we are grateful to E. W. Beier, W. Frati, and R. G. H. Robertson. The work of JNB is supported in part by NSF grant No. PHY95-13835. The work of EL was supported in part by the Institute for Advanced Study through a Hansmann fellowship, and in part by INFN. The research of EL was also performed under the auspices of the Theoretical Astroparticle Network, under contract No. CHRX-CT93-0120 of the Direction General XII of the E.E.C.

APPENDIX A: TESTING SNO BY MEASURING *IN SITU* ^8Li BETA-DECAY

The SNO collaboration plans to perform an overall test of the experiment by measuring the β -decay spectrum of an intense ^8Li source that will be placed in different locations in the detector. The measurement by SNO of the $^8\text{Li}(\beta^-)$ spectrum will be used as a demonstration that the results obtained for a known beta-decay spectrum are consistent with those measured in the laboratory.

Figure 9 compares our calculated (see below) ^8Li spectrum with the standard model electron spectrum from ^8B solar neutrino CC absorption [reaction (1)]. The test is based upon the fact that, despite the different physical processes that are involved in the two cases, the electron spectra from ^8Li β -decay and from ^8B solar neutrino absorption on deuterium have somewhat similar shapes and cover essentially the same energy range (from 0 to ~ 13 MeV). The spectra displayed in Fig. 9 are separately normalized to unity above the standard SNO threshold of 5 MeV and do not include broadening due to the finite energy resolution in the detector (or other signatures of the SNO detector).

We discuss in this appendix some of the things that can be learned from the ^8Li test. For background information, we first summarize in subsection A 1 the relations between the ^8Li and the ^8B electron spectra. We then describe in subsection A 2 how a future precision laboratory measurement of the ^8Li spectrum could be used, in conjunction with a SNO measurement of the ^8Li spectrum, to help determine characteristics of the SNO detector.

1. Relations Between the ^8Li and ^8B Spectra

The ^8Li electron spectrum is produced by the beta decay



The CC electron spectrum, whose measurement is one of the primary goals of SNO, is produced by a two-step reaction (beta decay followed by neutrino capture):



All three of these reactions are different, but the intermediate ^8Be states are the same in both ^8B (reaction A2a) and ^8Li (reaction A1) decay. The ^8Be excited states are unstable and break up into two alpha particles. As a consequence, the shape of the ^8Li β^- spectrum [Eq. (A2a)] and of the ^8B β^+ spectrum [Eq. (A2b)] deviate significantly from the standard allowed shape. The shape of the ^8B neutrino spectrum and its uncertainties are affected as well (see [6] and references therein).

Measurements of the delayed α spectrum allow one to determine the profile of the intermediate ^8Be state and thus to calculate the deviations of the ^8Li electron, ^8B positron, and ^8B neutrino spectra from their allowed shapes. The best-estimated ^8B positron and neutrino spectra and their uncertainties were discussed extensively in [6].

In Fig. 10a we show our best-estimate for the ${}^8\text{Li}(\beta^-)$ electron spectrum, together with its $\pm 3\sigma$ uncertainties. The calculation that leads to Fig. 10a is similar to the calculation of the ${}^8\text{B}(\beta^+)$ spectrum performed in [6], modulo different values for the radiative corrections, forbidden corrections, and Coulomb effects. The form factors entering the forbidden corrections are, by isospin symmetry, the same as used for ${}^8\text{B}(\beta^+)$ [6].

As discussed in Sec. II A, the 3σ uncertainties shown in Fig. 10a are related to a possible offset, b , in the energy of the α particles from ${}^8\text{Be}$ break-up: $E_\alpha \rightarrow E_\alpha + b$. The value of this offset affects, in particular, the calculated peaks of the β^+ , β^- , and ν spectra in Eqs. (A1) and (A2). The effective 3σ uncertainty of the offset b is estimated to be ± 0.104 MeV [6]; this estimate includes theoretical errors.

There are at least three complementary experiments that could help to reduce the offset uncertainty, b , and thereby make the prediction of the ${}^8\text{B}$ solar neutrino spectrum more precise. The potential experiments are: 1) a high-precision measurement of the α spectrum from ${}^8\text{Be}$ break-up; 2) a high-precision measurement of the β^+ spectrum from ${}^8\text{B}$ decay; and 3) a high-precision measurement of the β^- spectrum from ${}^8\text{Li}$ decay. In all three cases, dedicated laboratory experiments with a carefully calibrated spectrograph would be needed.

The SNO detector is expected to have an uncertainty in the absolute energy calibration of ~ 100 keV (1σ), and therefore probably cannot be used as a ${}^8\text{Li}$ spectrometer at the level of precision needed to further constrain b .

2. The SNO Response Function: $S_{\text{SNO}}(T'_e, T_e)$

In addition to an overall demonstration that the detector is working as expected, can one learn more about the characteristics of SNO by studying the $\text{Li}(\beta^-)$ spectrum? The answer is: “Yes, provided that a precision measurement of the ${}^8\text{Li}(\beta^-)$ spectrum is made with a laboratory spectrograph.” If future laboratory experiments determine accurately the ${}^8\text{Li}$ beta decay spectrum, then the measurement with SNO of this same spectrum can be used to constrain possible systematic effects that apply in the energy range that is also relevant for ${}^8\text{B}$ neutrino absorption ⁷.

Specifically, one could use the following strategy. Let $\lambda^{\text{Li}}(T'_e)$ be the *true* lithium spectrum as a function of the *true* electron energy, T'_e . Suppose, as a first approximation, that this spectrum is known with “infinite” precision as a result of an error-free laboratory spectrographic measurement:

$$\lambda_{\text{lab}}^{\text{Li}} \simeq \lambda^{\text{Li}}. \quad (\text{A3})$$

Then the lithium spectrum measured in the SNO detector, $\lambda_{\text{SNO}}^{\text{Li}}$, will be given by a convolution of $\lambda^{\text{Li}}(T'_e)$ with the SNO response function, $S_{\text{SNO}}(T'_e, T_e)$, where T_e is the *measured* electron kinetic energy and T'_e is the true electron energy. Thus

⁷ The theoretical ${}^8\text{Li}$ spectrum in Fig. 10a is affected by significant shape uncertainties (dotted lines) and is not a valid substitute for a high-precision laboratory measurement.

$$\lambda_{\text{SNO}}^{\text{Li}}(T_e) = \int \lambda^{\text{Li}}(T'_e) \cdot S_{\text{SNO}}(T'_e, T_e) dT'_e . \quad (\text{A4})$$

In our notation [see Eq. (13)], the SNO response function can be written as the product of the energy resolution and the CC detection efficiency:

$$S_{\text{SNO}}(T'_e, T_e) = R(T'_e, T_e) \cdot \epsilon_{\text{CC}}(T'_e) . \quad (\text{A5})$$

Therefore $S_{\text{SNO}}(T'_e, T_e)$ depends on three parameters: the energy resolution width σ_{10} [Eq. (8)], the absolute energy scale error δ [Eq. (9)], and the slope of the CC efficiency function β [Eq. (18)]. (Of course, other free parameters could be eventually introduced to model S_{SNO} more accurately.) Once λ^{Li} and $\lambda_{\text{SNO}}^{\text{Li}}$ are *experimentally* determined, one can use Eq. (A4) to fit the parameters of the SNO response function, S_{SNO} , which describes the spectral distortion effects induced by the detector. Since the SNO detector will also be calibrated with more traditional techniques (e.g., with γ rays of known energy), the determination of the free parameters in S_{SNO} will be overconstrained. The experimental overdetermination of S_{SNO} will limit the effects of unknown systematic errors. Moreover, the comparison of the fitted parameter values with those estimated by Monte Carlo simulations will provide further consistency checks.

In practice, one has to take account of uncertainties in the spectrum that is measured in the laboratory, $\lambda_{\text{lab}}^{\text{Li}}$, in order to infer the true spectrum λ^{Li} . The corrections will depend on the response function of the laboratory spectrograph, S_{lab} :

$$\lambda_{\text{lab}}^{\text{Li}}(T_e) = \int \lambda^{\text{Li}}(T'_e) \cdot S_{\text{lab}}(T'_e, T_e) dT'_e . \quad (\text{A6})$$

The response function S_{lab} must be known with a precision higher than what one hopes to achieve for the overall SNO response function, S_{SNO} . Any uncertainty, δS_{lab} , in the laboratory response function, will be propagated to S_{SNO} .

Are the available laboratory data on the $\text{Li}(\beta^-)$ decay sufficiently good that their uncertainties would not introduce large errors in the SNO response function if determined via Eq. (A4)? Unfortunately, the answer is “No.”

In Fig. 10b we show the published data from [45] and from [46], which are superimposed on the theoretical spectrum. (We have taken the data at face value and made no attempt to deconvolve resolution effects.) The agreement of the data with themselves and with the theoretical spectrum is unsatisfactory. In Fig. 10c, the β kinetic energies of each data set are linearly transformed, $T_\beta \rightarrow AT_\beta + B$, so that the two (renormalized) experimental spectra match each other and fit the theoretical spectrum. A good fit-by-eye (Fig. 10c) is obtained with parameters: $A = 0.94$, $B = 0.45$ MeV for the data of reference [45] and $A = 1.06$, $B = -0.2$ MeV for the data of reference [46]. The results of these transformations suggest that true spectrum, λ^{Li} , cannot be inferred from the available data with a precision better than a few hundred keV in the energy scale.

A new, precision laboratory measurement of the ${}^8\text{Li}(\beta^-)$ spectrum is needed.

APPENDIX B: STATISTICS OF LINEAR DEVIATIONS FROM THE STANDARD SPECTRUM

We state in the text that the average value of the electron kinetic energy, $\langle T \rangle$, is a good statistical estimator of *linear* deformations of the recoil spectrum. What we mean by this claim is that $\langle T \rangle$ contains most of the information about spectral deformations, especially if the deformations are small.

In this Appendix we show heuristically the basic correctness of the above statement in two simple but representative cases, purely statistical errors and a single dominant systematic error. More precisely, we show in Eq. (B8) (stat. error) and Eq. (B9) (syst. error) that, for a linear spectral deformation, the χ^2 associated with deviations of $\langle T \rangle$ is approximately equal to the χ^2 obtained by binning the observed spectrum in a histogram. However, if there are several comparable systematic errors, or if the deviation is nonlinear, significant additional information may be obtained from the higher moments [41].

The arguments given below are in the spirit of a “physicist’s proof” rather than a mathematical theorem. We note that for probability distributions with long tails the analysis in terms of moments may not be appropriate. Fortunately, the spectrum of electron recoil energies does not have pathologically long tails so this last remark does not apply in the case we are considering.

Let $\rho(T)$ be the *expected* normalized electron recoil spectrum [$\int dT \rho(T) = 1$], with average kinetic energy $\langle T \rangle$ and variance σ^2 . Let $\rho'(T)$ be the *observed* normalized spectrum, with average energy $\langle T \rangle'$. In the hypothesis of a perfectly linear spectral deformation, one can always write:

$$\frac{\rho'(T)}{\rho(T)} = 1 + \beta \frac{T - \langle T \rangle}{\langle T \rangle}, \quad (\text{B1})$$

where β is a slope parameter. Then the shift in the average energy is given by

$$\Delta \langle T \rangle \equiv \langle T \rangle' - \langle T \rangle = \beta \frac{\sigma^2}{\langle T \rangle}, \quad (\text{B2})$$

and its χ^2 statistic simply reads

$$\chi_{\langle T \rangle}^2 = \left(\frac{\Delta \langle T \rangle}{\sigma_{\langle T \rangle}} \right)^2, \quad (\text{B3})$$

where $\sigma_{\langle T \rangle}$ is the total error affecting $\langle T \rangle$.⁸

⁸ Notice from Eq. (B2) that $\Delta \langle T \rangle$ and β are in one-to-one correspondence, so that a determination of the shift in the average energy $\langle T \rangle$ is equivalent to a determination of the slope of $\rho'(T)/\rho(T)$ with the same fractional accuracy, and vice versa. The observables $\Delta \langle T \rangle$ and β are interchangeable for a linear spectral distortion. We prefer $\Delta \langle T \rangle$ because the average kinetic energy is well-defined also in the case of a non-linear distortion, while β is not.

For purely statistical errors, $\sigma_{\langle T \rangle}^2 = \sigma^2/N$ by the central limit theorem, where N is the total number of observed electrons. From Eqs. (B2) and (B3) one has:

$$\chi_{\langle T \rangle}^2 = \beta^2 \frac{\sigma^2}{\langle T \rangle^2} N \quad (\text{stat. dominated}) . \quad (\text{B4})$$

A single small, purely systematic error (such as the uncertainty in the ^8B neutrino spectrum shape or in the absolute energy calibration) also produces, in first order, a linear deformation of the expected recoil spectrum. The spectral distortion can thus be represented as an uncertainty σ_β of the slope parameter β . Then, from Eq. (B2), the propagated error on $\langle T \rangle$ is $\sigma_{\langle T \rangle} = \sigma_\beta \sigma^2 / \langle T \rangle$, and one has from Eqs. (B2) and (B3):

$$\chi_{\langle T \rangle}^2 = \frac{\beta^2}{\sigma_\beta^2} \quad (\text{syst. dominated}) , \quad (\text{B5})$$

as would be expected intuitively.

Let us divide now the spectra in n bins of width ΔT_i : $\rho \equiv \{\rho_i, \Delta T_i\}_{i=1, \dots, n}$ and $\rho' \equiv \{\rho'_i, \Delta T_i\}_{i=1, \dots, n}$, with $\sum_i \rho_i \Delta T_i = \sum_i \rho'_i \Delta T_i = 1$. Then the shift in the height of the i -th bin associated to the linear deformation in Eq. (B1) is:

$$\Delta \rho_i \equiv \rho'_i - \rho_i = \rho_i \beta \frac{T_i - \langle T \rangle}{\langle T \rangle} , \quad (\text{B6})$$

where T_i is the average value of T in the i -th bin.

If counting statistics dominates the errors, the fractional uncertainty σ_i/ρ_i of the i -th bin height is $\sigma_i/\rho_i = 1/\sqrt{N\rho_i\Delta T_i}$, and the total χ^2 of the histogram differences, $\chi_{\text{hist}}^2 = \sum_i (\Delta \rho_i/\sigma_i)^2$, is easily derived:

$$\chi_{\text{hist}}^2 = \beta^2 \frac{\hat{\sigma}^2}{\langle T \rangle^2} N , \quad (\text{B7})$$

where $\hat{\sigma}^2 = \sum_i \rho_i \Delta T_i (T_i - \langle T \rangle)^2$ is just a discretized estimate of the variance σ^2 , and therefore $\hat{\sigma}^2 \simeq \sigma^2$. One gets the desired proof by comparing Eqs. (B4) and (B7):

$$\chi_{\text{hist}}^2 \simeq \chi_{\langle T \rangle}^2 \quad (\text{stat. dominated}) . \quad (\text{B8})$$

If systematic errors dominate, the corresponding analysis of a binned spectrum is somewhat trickier. Let the error be represented by an overall uncertainty σ_β of the slope parameter β . From Eq. (B6), this uncertainty propagates to an error $\sigma_i = \sigma_\beta \rho_i (T_i - \langle T \rangle) / \langle T \rangle$ of the i -th bin. The formula $\chi_{\text{hist}}^2 = \sum_i (\Delta \rho_i/\sigma_i)^2$ naively (and incorrectly) applied to this case would give $\chi_{\text{hist}}^2 = n\beta^2/\sigma_\beta^2 = n\chi_{\langle T \rangle}^2$, with $\chi_{\langle T \rangle}^2$ given by Eq. (B5). However, a systematic shift in the slope β produces completely correlated bin errors: $\text{corr}(i, j) = 1$. Therefore, only one out the n bin residuals is independent, and the ‘‘effective’’ number of bins to be considered in the χ^2 is 1⁹, so that $\chi_{\text{hist}}^2 = \beta^2/\sigma_\beta^2$ and:

⁹The reader more experienced in statistical analyses may have noticed that, in this case, the square error matrix including the error correlations would have rank 1 and not n , signaling that only one bin error is independent.

$$\chi_{\text{histo}}^2 = \chi_{\langle T \rangle}^2 \quad (\text{syst. dominated}) . \quad (\text{B9})$$

Equations (B8) and (B9) show that, if the errors are dominated by statistics or by a single systematic uncertainty, the use of the integrated variable $\langle T \rangle$ is as informative as a spectrum histogram, provided that the spectral deformations are linear in T .

REFERENCES

- [1] SNO Collaboration, G. T. Ewan *et al.*, “Sudbury Neutrino Observatory Proposal,” Report No. SNO-87-12, 1987 (unpublished); “Scientific and Technical Description of the Mark II SNO Detector,” edited by E. W. Beier and D. Sinclair, Report No. SNO-89-15, 1989 (unpublished). A. B. McDonald, Proceedings of the 9th Lake Louise Winter Institute, edited by A. Astbury *et al.* (World Scientific, Singapore, 1994), p. 1.
- [2] S. L. Glashow, Nucl. Phys. **22**, 579 (1961); S. Weinberg, Phys. Rev. Lett. **19**, 1264 (1967); A. Salam, in *Elementary Particle Theory*, edited by N. Svartholm (Almqvist and Wiksells, Stockholm, 1968), p. 367.
- [3] Particle Data Group, L. Montanet *et al.*, Phys. Rev. D **50**, 1173 (1994).
- [4] J. N. Bahcall, Phys. Rev. D **44**, 1644 (1991).
- [5] H. H. Chen, Phys. Rev. Lett. **55**, 1534 (1985).
- [6] J. N. Bahcall, E. Lisi, D. E. Alburger, L. De Braeckelee, S. J. Freedman, and J. Napolitano, Institute for Advanced Study Report No. IASSNS-AST 95/47, e-print archive No. nucl-th/9601044, to appear in Phys. Rev. C.; see also: J. N. Bahcall and B. R. Holstein, Phys. Rev. C **33**, 2121 (1986).
- [7] J. N. Bahcall, N. Cabibbo, and A. Yahil, Phys. Rev. Lett. **28**, 316 (1972).
- [8] Z. G. Berezhiani and M. I. Vysotsky, Phys. Lett. B **199**, 281 (1987).
- [9] M. B. Voloshin, M. I. Vysotskii, and L. B. Okun, Soviet Phys. JETP **64**, 446 (1986); **65**, 209(E) (1987).
- [10] C.-S. Lim and W. J. Marciano, Phys. Rev. D **37**, 1368 (1988).
- [11] E. K. Akhmedov, Phys. Lett. B **213**, 64 (1988).
- [12] M. Gasperini, Phys. Rev. D **38**, 2635 (1988).
- [13] E. Roulet, Phys. Rev. D **44**, R935 (1991).
- [14] M. M. Guzzo, A. Masiero, and S. T. Petcov, Phys. Lett. B **260**, 154 (1991).
- [15] J. N. Bahcall, R. Davis, Jr., P. Parker, A. Smirnov, and R. Ulrich, editors: *Solar Neutrinos, The First Thirty Years*, Frontiers in Physics, Vol. 92 (Addison-Wesley, 1994).
- [16] Updated information on the status of the SNO experiment can be retrieved from the following URL: <http://snodaq.phy.queensu.ca/SNO/sno.html>.
- [17] J. N. Bahcall, *Neutrino Astrophysics* (Cambridge University Press, Cambridge, England, 1989).
- [18] P. I. Krastev and A. Yu. Smirnov, Phys. Lett. B **338**, 282 (1994); N. Hata and P. Langacker, Phys. Rev. D **50**, 632 (1994); P. I. Krastev and S. T. Petcov, Nucl. Phys. **B449**, 605 (1995).
- [19] G. Fiorentini, M. Lissia, G. Mezzorani, M. Moretti, and D. Vignaud, Phys. Rev. D **49**, 6298 (1994).
- [20] W. Kwong and S. P. Rosen, Phys. Rev. D **51**, 6159 (1995); see also Phys. Rev. Lett. **68**, 748 (1992).
- [21] SNO collaboration, Internal Report (unpublished).
- [22] J. Napolitano, S. J. Freedman, and J. Camp, Phys. Rev. C **36**, 298 (1987).
- [23] D. H. Wilkinson and D. E. Alburger, Phys. Rev. Lett. **26**, 1127 (1971); numerical data tables are reported in E. K. Warburton, Phys. Rev. C **33**, 303 (1986).
- [24] J. N. Bahcall and M. H. Pinsonneault, Rev. Mod. Phys. **64**, 885 (1992).
- [25] J. N. Bahcall and M. H. Pinsonneault, Rev. Mod. Phys. **67**, (1995) 781.

- [26] T. L. Jenkins, “A Proposed Experiment for the Detection of Solar Neutrinos,” Case Western Reserve Univ. Report No. C00-818-62, 1962 (unpublished).
- [27] K. Kubodera and S. Nozawa, *Int. J. Mod. Phys. E* **3**, 101 (1994).
- [28] Yu. S. Kopysov and V. A. Kuz'min, *Yad. Fiz.* **4**, 1031 (1966) [*Sov. J. Nucl. Phys.* **4**, 740 (1967)].
- [29] F. J. Kelly and H. Überall, *Phys. Rev. Lett.* **16**, 145 (1966).
- [30] S. D. Ellis and J. N. Bahcall, *Nucl. Phys.* **A114**, 636 (1968).
- [31] H. A. Bethe, *Phys. Rev.* **76**, 38 (1949); H. A. Bethe and C. Longmire, *Phys. Rev.* **77**, 647 (1950).
- [32] S. Ying, W. C. Haxton, and E. M. Henley, *Phys. Rev. C* **45**, 1982 (1992).
- [33] M. Doi and K. Kubodera, *Phys. Rev. C* **45**, 1988 (1992).
- [34] M. A. Preston and R. K. Bhaduri, *Structure of the Nucleus* (Addison-Wesley, 1975, Reading, Massachusetts).
- [35] S. M. Bilenky and C. Giunti, *Phys. Lett. B* **311**, 179 (1993).
- [36] J. N. Bahcall, K. Kubodera, and S. Nozawa, *Phys. Rev. D* **38**, 1030 (1988).
- [37] J. N. Bahcall, *Phys. Rev. Lett.* **23**, 251 (1969).
- [38] Kamiokande collaboration, K. S. Hirata *et al.*, *Phys. Rev. D* **44**, 2241 (1991).
- [39] G. Beier, private communication (1996); A. Hallin, private communication (1996).
- [40] R. G. H. Robertson, private communication (1996).
- [41] J. N. Bahcall, P. I. Krastev, and E. Lisi, in preparation.
- [42] L. Wolfenstein, *Phys. Rev. D* **17**, 2369 (1978); S. P. Mikheyev and A. Yu. Smirnov, *Yad. Fiz.* **42**, 1441 (1985) [*Sov. J. Nucl. Phys.* **42**, 913 (1985)].
- [43] V. N. Gribov and B. M. Pontecorvo, *Phys. Lett. B* **28**, 493 (1969); J. N. Bahcall and S. C. Frautschi, *Phys. Lett. B* **29**, 623 (1969); S. L. Glashow and L. M. Krauss, *Phys. Lett. B* **190**, 199 (1987).
- [44] J. N. Bahcall and P. I. Krastev, *Phys. Rev. D* **53**, 4211 (1996).
- [45] W. F. Hornyak and T. Lauritsen, *Phys. Rev.* **77**, 160 (1950).
- [46] M. Allet *et al.*, *Phys. Rev. Lett.* **68**, 572; see also J. Sromicki *et al.*, *Phys. Rev. C* **53**, 932 (1996).

TABLES

TABLE I. The percentage 1σ errors from different ingredients that affect the standard predictions, $\langle T_e \rangle = 7.658$ MeV and $R_{CC}/R_{NC} = 1.882$. The numbers given are for $N_{CC} = 5000$ events above threshold ($T_{\min} = 5$ MeV), and $\epsilon_{CC} = 1$, $\epsilon_{NC} = 0.5$. Uncertainties due to the backgrounds are neglected. The approximate cancellation of the correlation of total the errors may not be as strong for the actual SNO error budget.

Error component	$\sigma(\langle T_e \rangle)$ %	$\sigma(R_{CC}/R_{NC})$ %	Correlation
Neutrino spectrum	0.38	0.43	+1
Cross section	0.14	0.53	~ 0
Statistics	0.33	3.09	0
Energy resolution	0.31	0.47	-1
Energy scale	0.68	1.81	+1
Efficiency	~ 0	2.00	~ 0
TOTAL	0.91	4.18	0.32

TABLE II. Deviations of $\langle T_e \rangle$ and R_{CC}/R_{NC} from the standard model (electron flavor conserved) predictions. The results are shown for representative neutrino oscillation scenarios in units of standard deviations (σ). In the last two columns, the combined χ^2 for the CC-shape and CC/NC ratio tests is calculated with and without the correlation of the total errors ($\rho = 0.32$), and the deviation is given as: Dev. (σ) = $\sqrt{\chi^2}$. Uncertainties due to the backgrounds are neglected.

Scenario	Acronym	CC-shape test		CC/NC test		Combined tests	
		$\langle T_e \rangle$ (MeV)	Dev. (σ)	R_{CC}/R_{NC}	Dev. (σ)	$\rho = 0.22$	$\rho = 0$
Standard	STD	7.658	—	1.882	—	—	—
Small Mixing Angle (MSW)	SMA	7.875	3.1	0.639	15.7	17.9	16.0
Large Mixing Angle (MSW)	LMA	7.654	0.0	0.422	18.5	19.5	18.5
Vacuum Oscillations	VAC	8.361	10.0	0.411	18.6	25.1	21.1

TABLE III. The dependence of $\langle T_e \rangle$, R_{CC}/R_{NC} , and of their errors, on the threshold energy, T_{\min} . The correlation of errors is given in the last column. The results shown assume 5000 CC events collected above threshold. Uncertainties due to the backgrounds are neglected. The acronyms for the scenarios (STD, SMA, LMA, VAC) are the same as in Table II.

T_{\min} (MeV)	Average energy $\langle T_e \rangle$ (MeV)				CC/NC ratio, R_{CC}/R_{NC}				Correlation
	STD $\pm 1\sigma$	SMA	LMA	VAC	STD $\pm 1\sigma$	SMA	LMA	VAC	ρ
4.0	7.234 ± 0.079	7.533	7.228	8.101	2.177 ± 0.088	0.712	0.489	0.440	0.23
5.0	7.658 ± 0.070	7.875	7.654	8.361	1.882 ± 0.079	0.639	0.422	0.411	0.32
6.0	8.187 ± 0.063	8.337	8.184	8.678	1.509 ± 0.067	0.534	0.338	0.369	0.43
7.0	8.798 ± 0.058	8.897	8.796	9.110	1.107 ± 0.056	0.409	0.248	0.307	0.52

TABLE IV. The energy threshold (T_{\min}) dependence of the deviations, ξ , of the predictions with neutrino oscillations from the standard predictions. The entries in the table, $\xi(\langle T_e \rangle)$ and $\xi(R_{CC}/R_{NC})$, are in units of standard deviations. The acronyms for the oscillation scenarios (SMA, LMA, VAC) are the same as in Table II. Uncertainties due to the backgrounds are neglected.

T_{\min} (MeV)	$\xi(\langle T_e \rangle)$			$\xi(R_{CC}/R_{NC})$			Combined, $\xi = \sqrt{\chi^2}$		
	SMA	LMA	VAC	SMA	LMA	VAC	SMA	LMA	VAC
4.0	3.8	0.1	11.0	16.6	19.2	19.7	18.3	19.8	25.4
5.0	3.1	0.0	10.0	15.7	18.5	18.6	17.5	19.5	25.1
6.0	2.4	0.0	7.8	14.6	17.4	17.0	17.4	19.2	23.9
7.0	1.7	0.0	5.4	12.5	15.3	14.3	15.8	17.9	20.7

TABLE V. The CC event rates as a function of the CC energy threshold and the neutrino oscillation solution.

T_{\min} (MeV)	STD (SNU)	SMA (SNU)	LMA (SNU)	VAC (SNU)
4	6.9	2.3	1.6	1.4
5	6.0	2.0	1.3	1.3
6	4.8	1.7	1.1	1.2
7	3.5	1.3	0.8	1.0

FIGURES

FIG. 1. (a) Total CC cross section as calculated by Kubodera and Nozawa (KN), Ying, Haxton and Henley (YHH), and Ellis and Bahcall (EB), slightly improved. (b) Total NC cross section as calculated by Kubodera and Nozawa (KN), and Ying, Haxton and Henley (YHH).

FIG. 2. Comparison of the CC differential cross-section at various energies and scattering angles. Solid: Kubodera and Nozawa [27]. Dotted: Ellis and Bahcall [30], slightly improved.

FIG. 3. The normalized electron spectrum, with and without inclusion of the energy resolution function.

FIG. 4. Three standard deviation departures from the standard electron spectrum (solid line) due to neutrino-related and detector-related errors.

FIG. 5. Neutrino Oscillation Scenarios: (a) survival probabilities for oscillation test cases; (b) effect of neutrino oscillations on neutrino spectrum at earth; (c) effect of neutrino oscillations on normalized electron spectrum at SNO. Area under curves = 1; (d) effect of neutrino oscillations on electron spectrum at SNO. Area under curves = N_{CC}/N_{NC} . Labels: STD = standard (no oscillation); SMA = small mixing angle (MSW); LMA = large mixing angle (MSW); VAC = vacuum oscillation. See the text for details.

FIG. 6. Ratios of the normalized neutrino spectra for different oscillation scenarios. The normalized spectra are displayed in Fig. 5c. Labels as in Fig. 5.

FIG. 7. Values of the characteristic CC-shape variable, the average energy $\langle T_e \rangle$, and of the CC/NC ratio, R_{CC}/R_{NC} , together with 3σ error bars. Uncertainties due to the backgrounds are neglected. Labels as in Fig. 5.

FIG. 8. Iso-sigma contours ($\sigma = \sqrt{\chi^2}$) for the combined CC-shape and CC/NC test, for the representative oscillation cases shown in Fig. 5 and discussed in the text. Uncertainties due to the backgrounds are neglected. For values of the iso-sigma distance $\mathcal{N}(\sigma) \gg 3$, the number of standard deviations is only a formal characterization; the tail of the probability distribution is not expected to be Gaussian for very large values of $\mathcal{N}(\sigma)$. Labels as in Fig. 5.

FIG. 9. A comparison of the ${}^8\text{Li}$ beta-decay spectrum and the standard electron spectrum from ${}^8\text{B}$ neutrino absorption, as a function of the electron kinetic energy above the standard SNO threshold (5 MeV). The spectra shown are both theoretical: the effects of finite energy resolution are not included. The area under the curves is normalized to unity.

FIG. 10. (a) Theoretical ${}^8\text{Li}$ spectrum and its 3σ uncertainties. (b) Experimental determinations of the ${}^8\text{Li}$ spectrum. (c) Experimental data with an allowance for a linear recalibration of the energy. See the text for details.

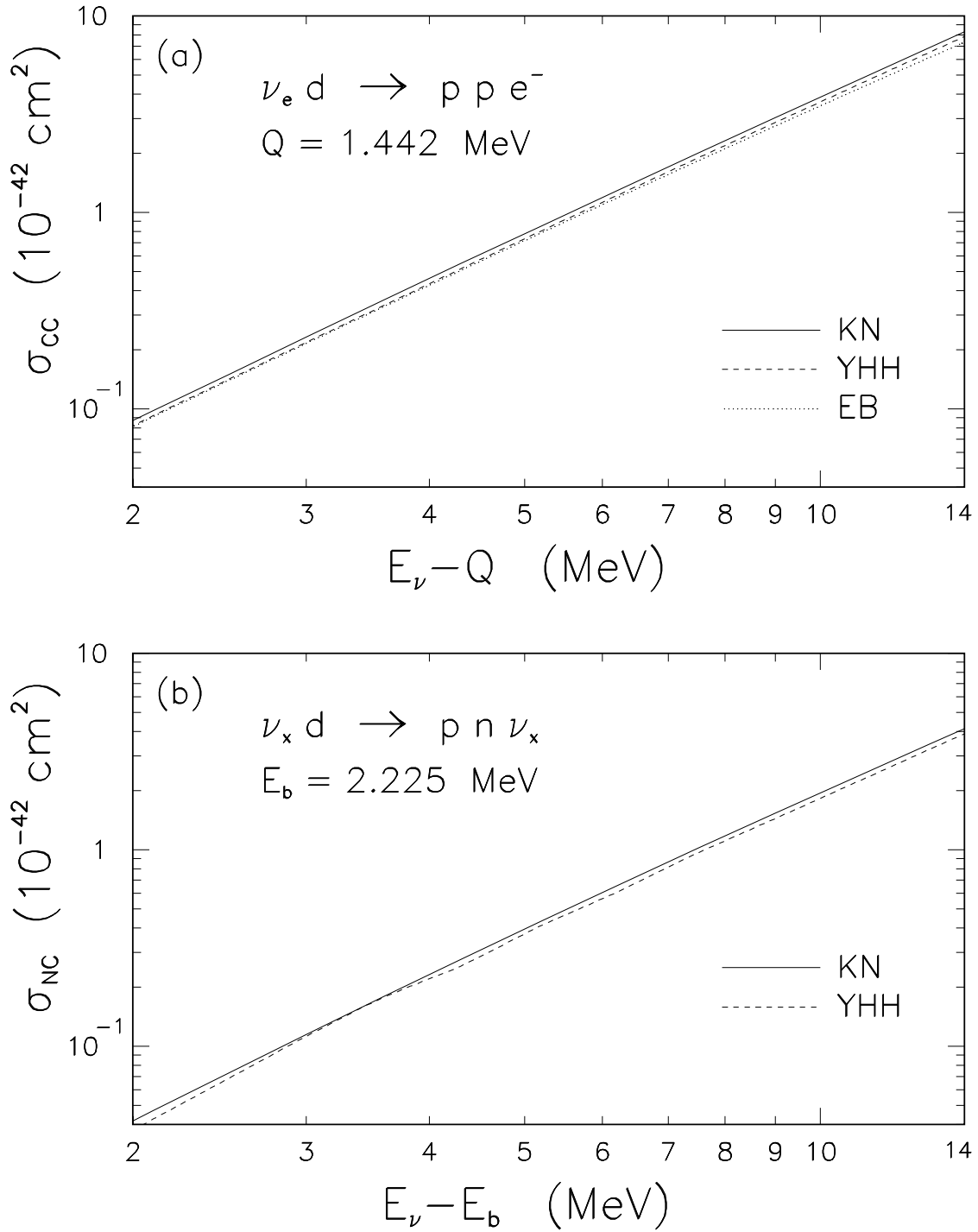


FIG. 1. (a) Total CC cross section as calculated by Kubodera and Nozawa (KN), Ying, Haxton and Henley (YHH), and Ellis and Bahcall (EB), slightly improved. (b) Total NC cross section as calculated by Kubodera and Nozawa (KN), and Ying, Haxton and Henley (YHH).

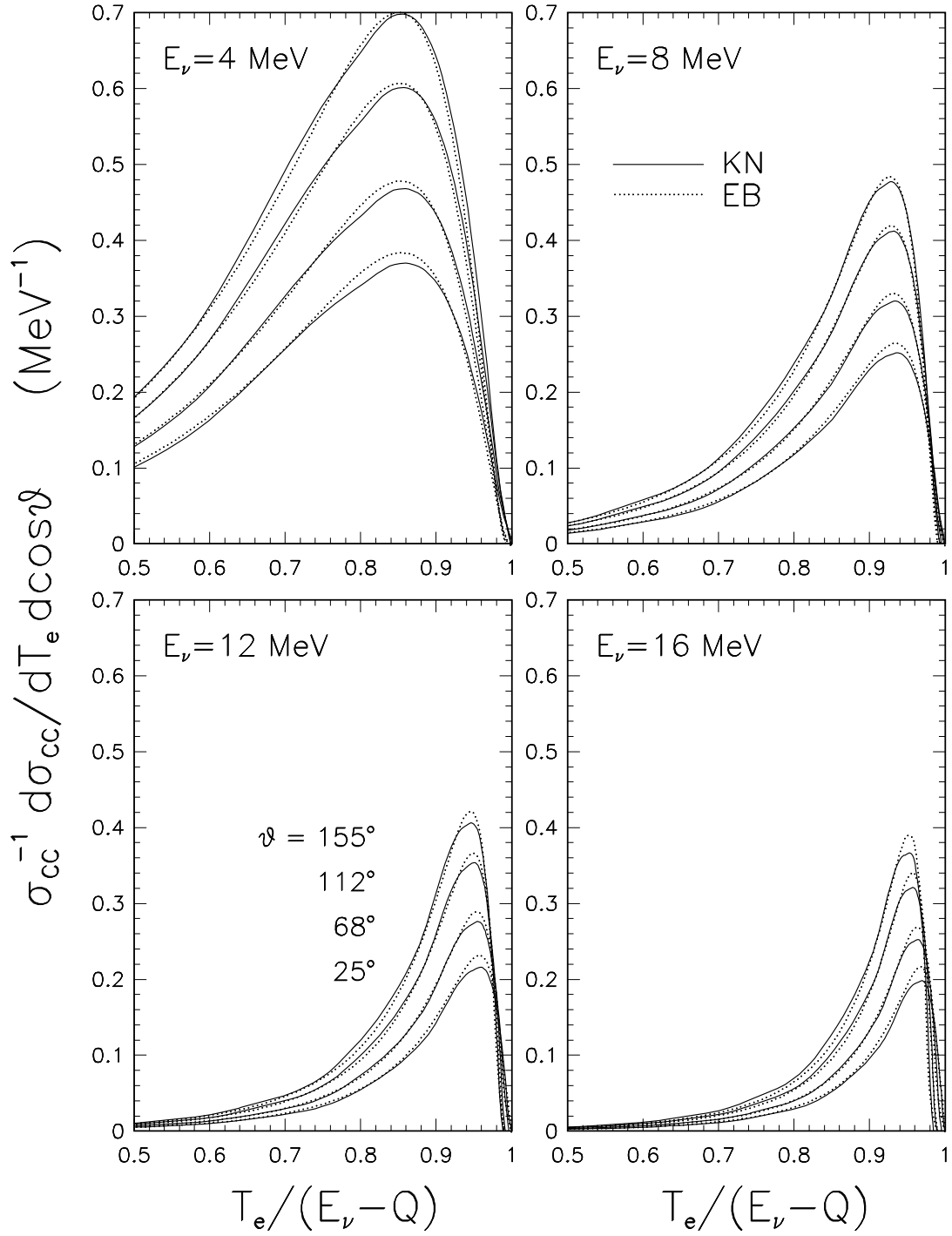


FIG. 2. Comparison of the CC differential cross-section at various energies and scattering angles. Solid: Kubodera and Nozawa [27]. Dotted: Ellis and Bahcall [30], slightly improved.

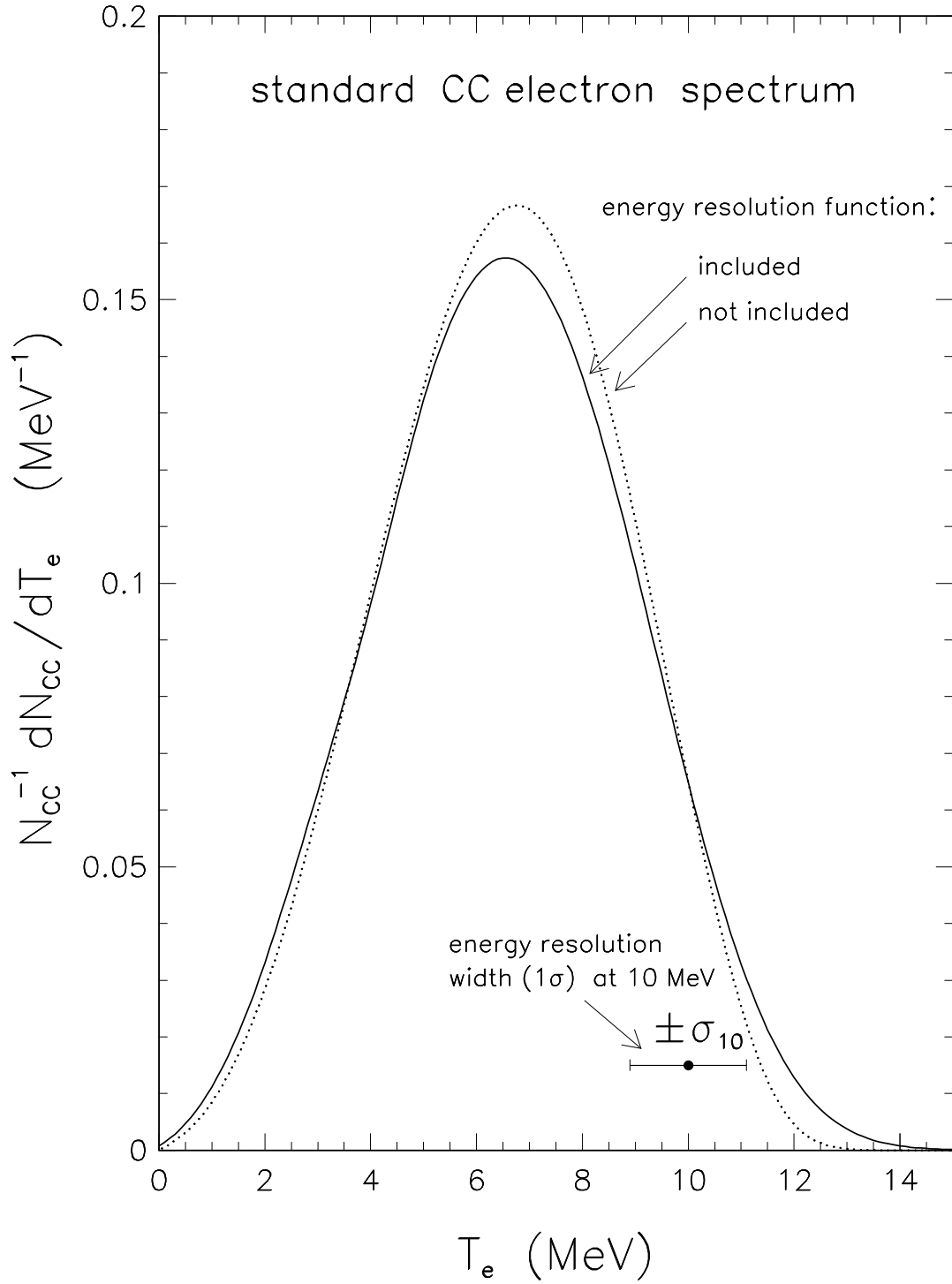


FIG. 3. The normalized electron spectrum, with and without inclusion of the energy resolution function.

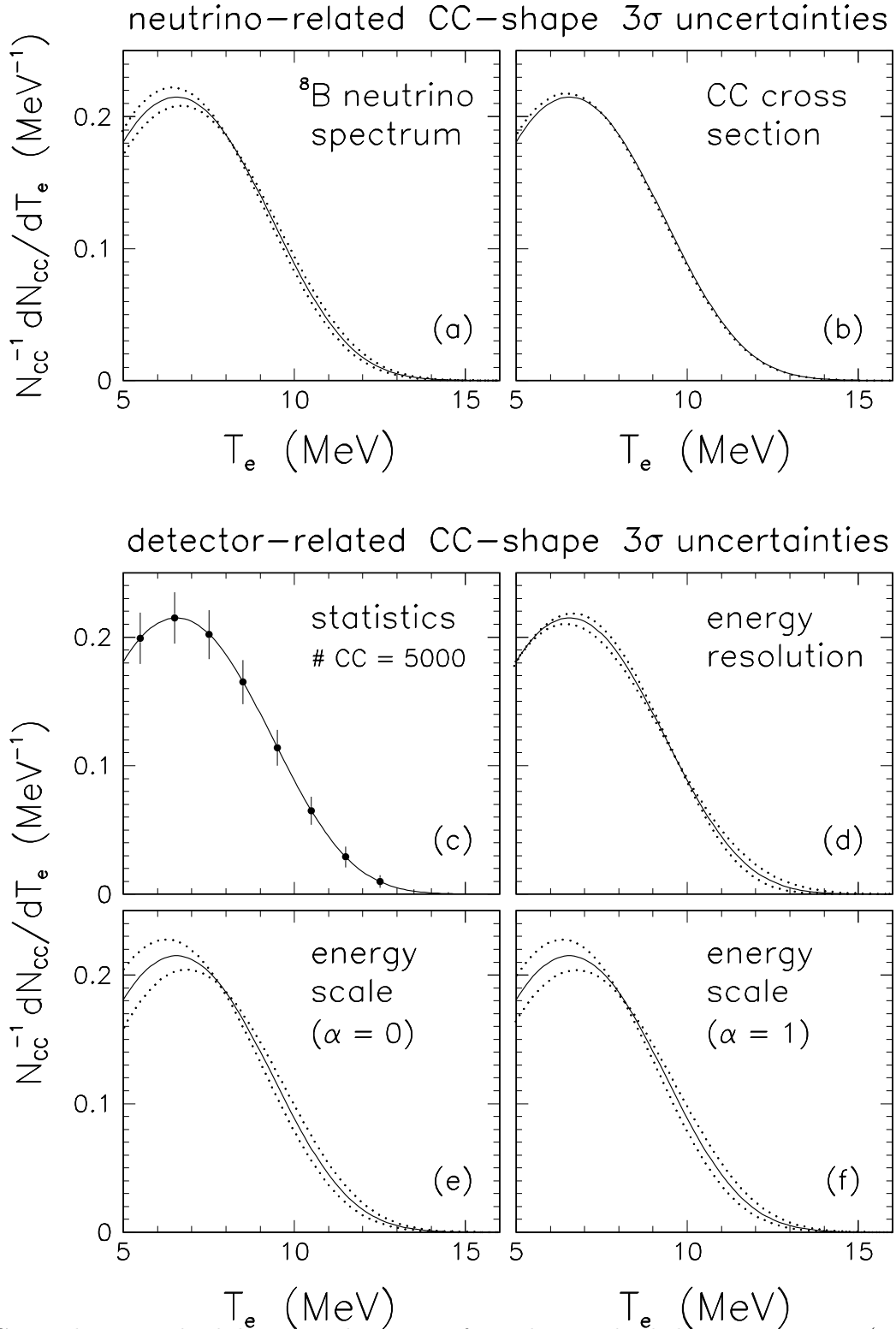


FIG. 4. Three standard deviation departures from the standard electron spectrum (solid line) due to neutrino-related and detector-related errors.

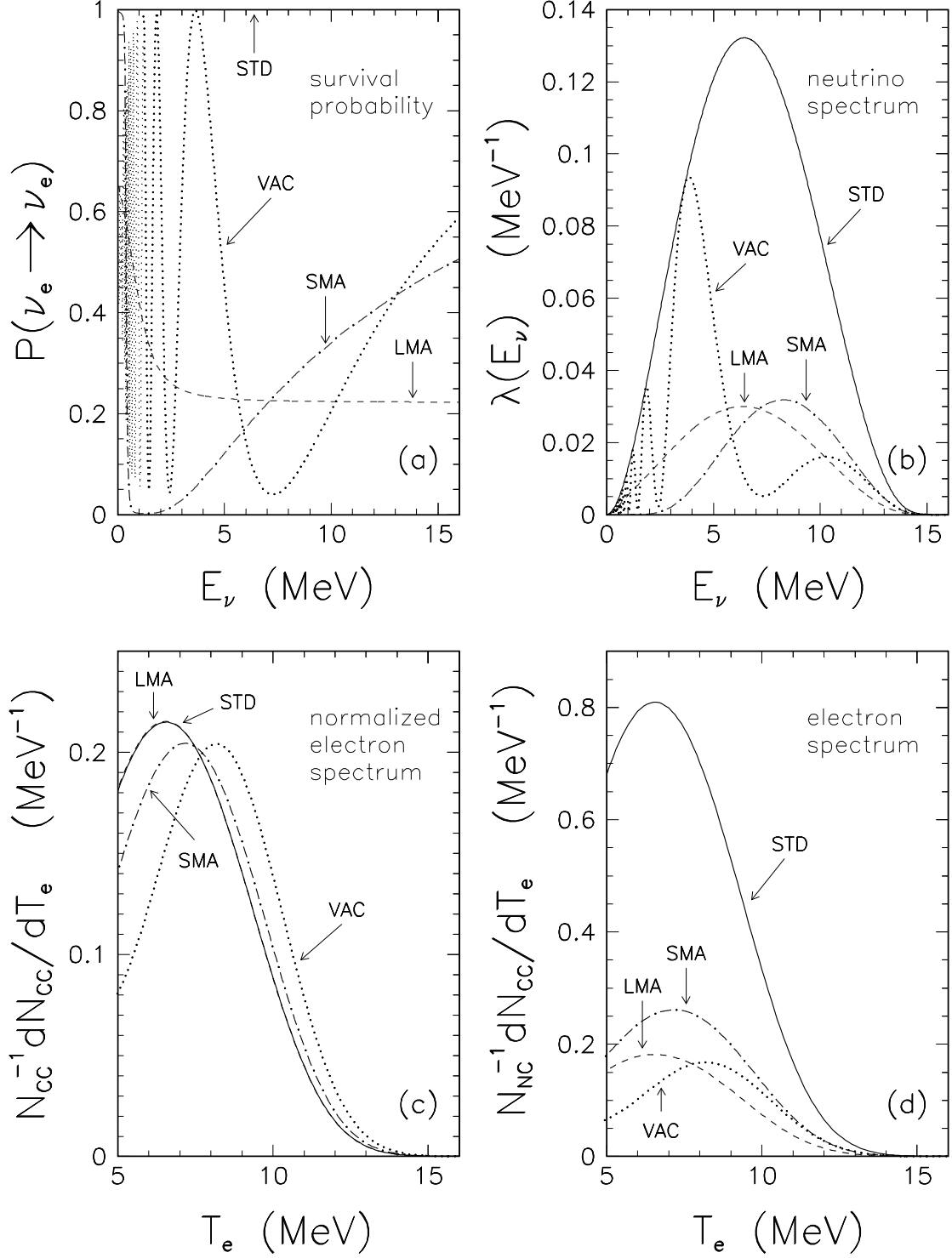


FIG. 5. Neutrino Oscillation Scenarios: (a) survival probabilities for oscillation test cases; (b) effect of neutrino oscillations on neutrino spectrum at earth; (c) effect of neutrino oscillations on normalized electron spectrum at SNO. Area under curves = 1; (d) effect of neutrino oscillations on electron spectrum at SNO. Area under curves = N_{CC}/N_{NC} . Labels: STD = standard (no oscillation); SMA = small mixing angle (MSW); LMA = large mixing angle (MSW); VAC = vacuum oscillation. See the text for details.

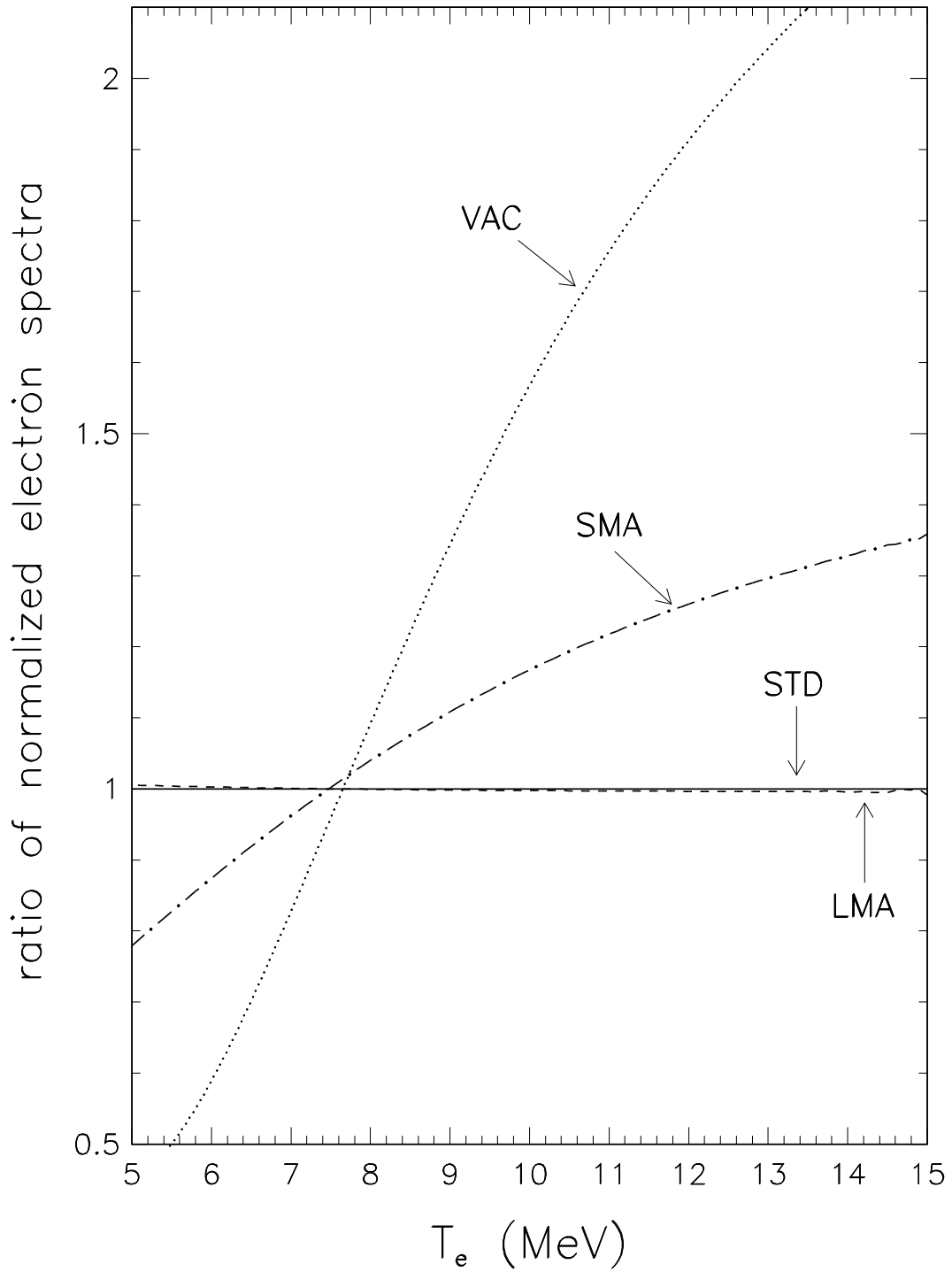


FIG. 6. Ratios of the normalized neutrino spectra for different oscillation scenarios. The normalized spectra are displayed in Fig. 5c. Labels as in Fig. 5.

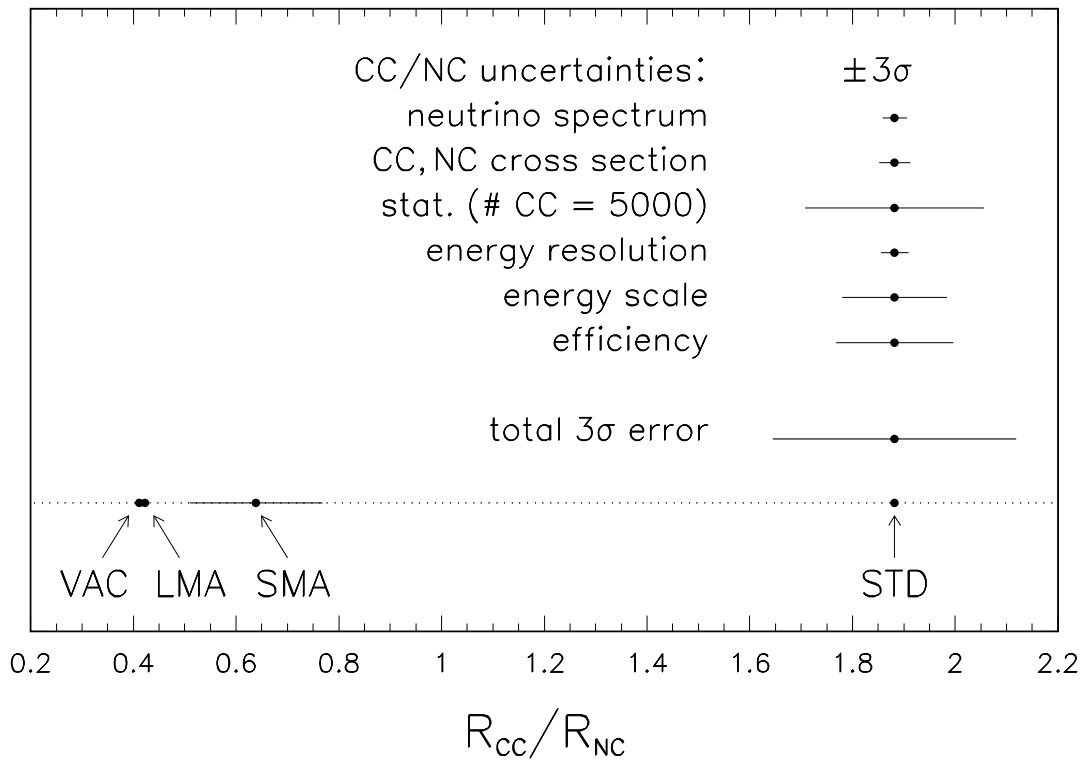
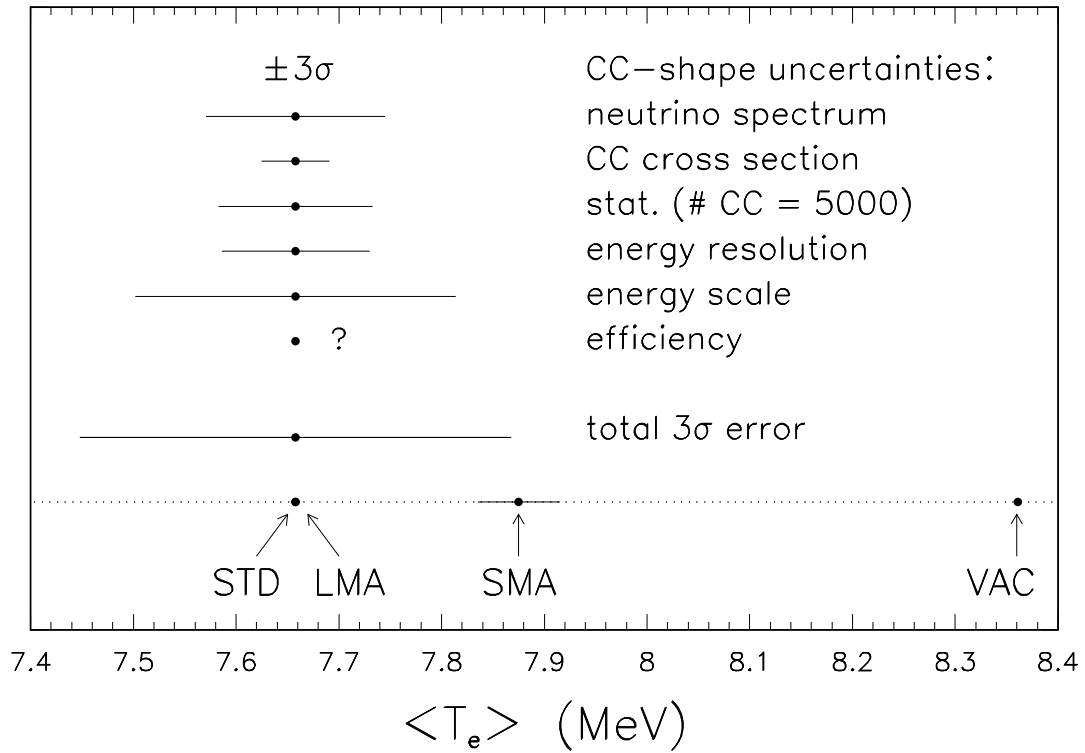


FIG. 7. Values of the characteristic CC-shape variable, the average energy $\langle T_e \rangle$, and of the CC/NC ratio, R_{CC}/R_{NC} , together with 3σ error bars. Uncertainties due to the backgrounds are neglected. Labels as in Fig. 5.

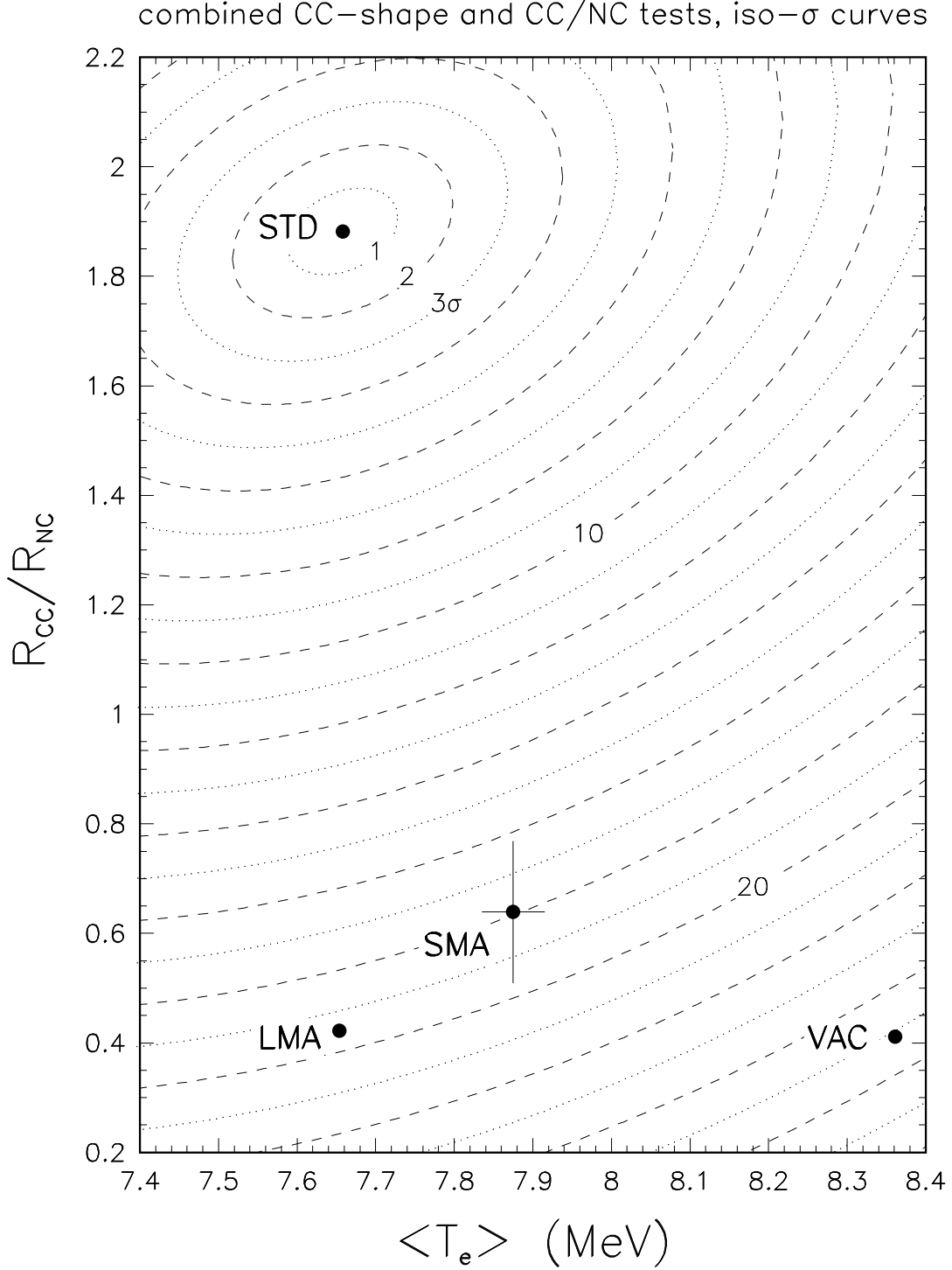


FIG. 8. Iso-sigma contours ($\sigma = \sqrt{\chi^2}$) for the combined CC–shape and CC/NC test, for the representative oscillation cases shown in Fig. 5 and discussed in the text. Uncertainties due to the backgrounds are neglected. For values of the iso-sigma distance $\mathcal{N}(\sigma) \gg 3$, the number of standard deviations is only a formal characterization; the tail of the probability distribution is not expected to be Gaussian for very large values of $\mathcal{N}(\sigma)$. Labels as in Fig. 5.

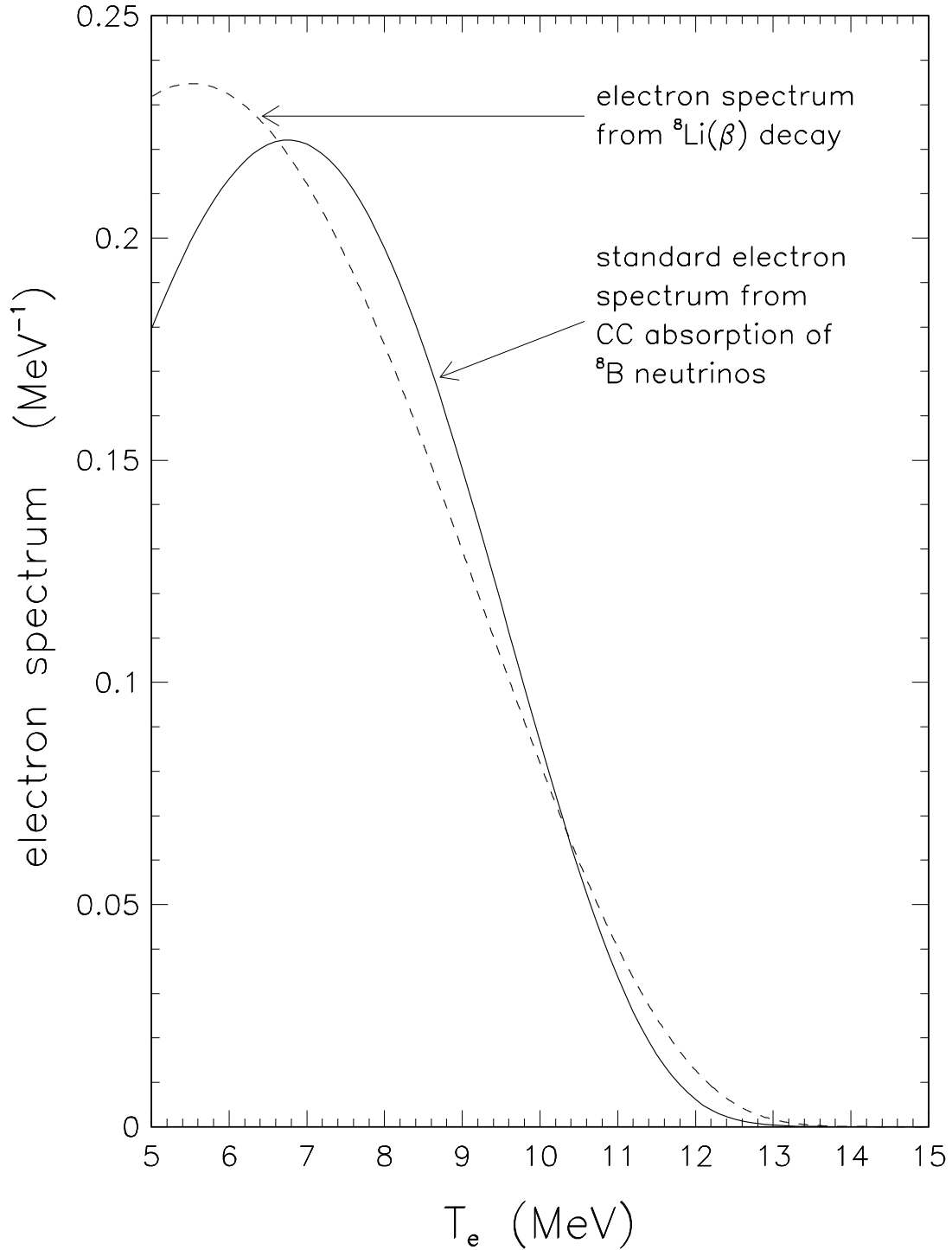


FIG. 9. A comparison of the ${}^8\text{Li}$ beta-decay spectrum and the standard electron spectrum from ${}^8\text{B}$ neutrino absorption, as a function of the electron kinetic energy above the standard SNO threshold (5 MeV). The spectra shown are both theoretical: the effects of finite energy resolution are not included. The area under the curves is normalized to unity.

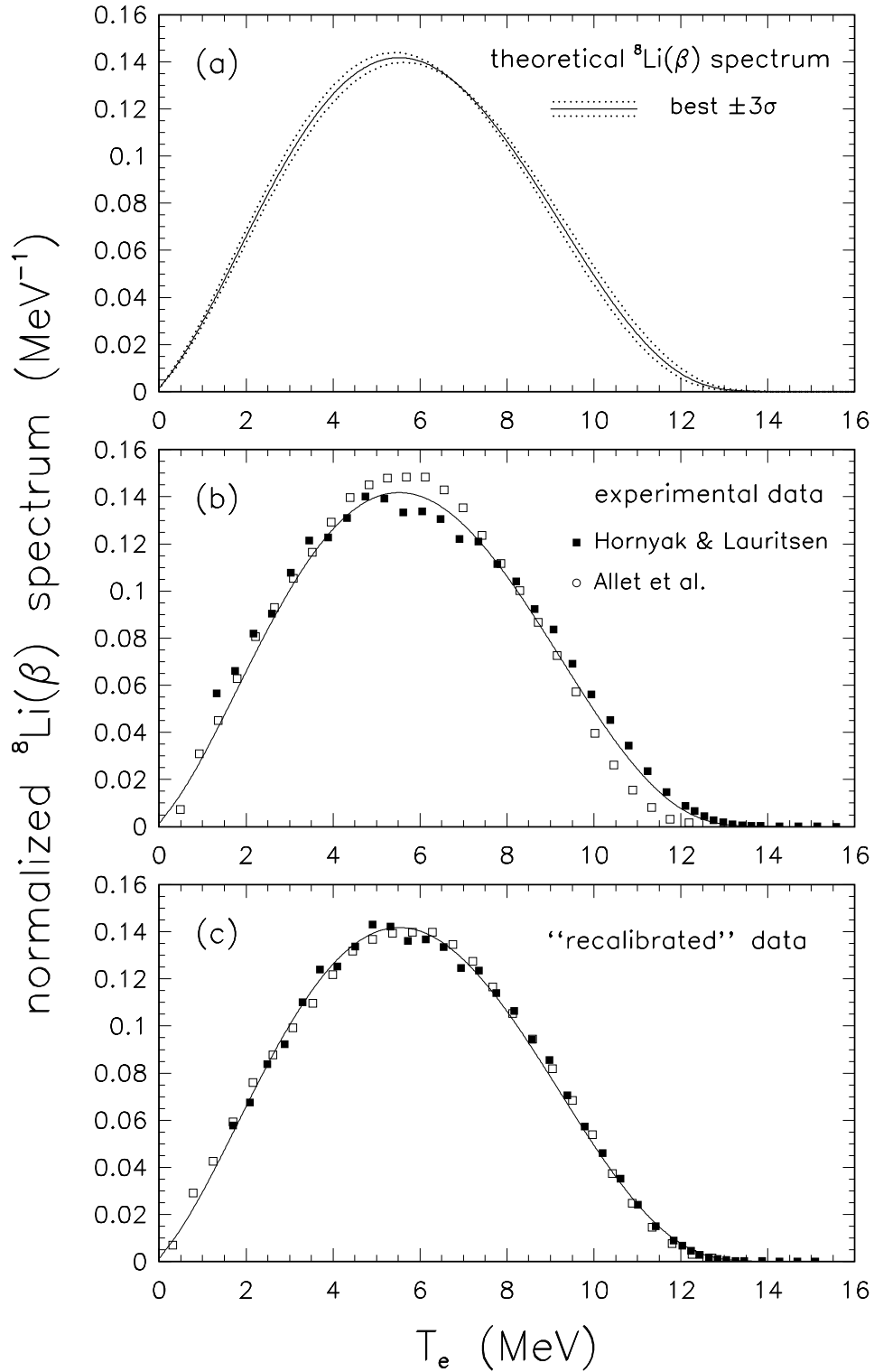


FIG. 10. (a) Theoretical ${}^8\text{Li}$ spectrum and its 3σ uncertainties. (b) Experimental determinations of the ${}^8\text{Li}$ spectrum. (c) Experimental data with an allowance for a linear recalibration of the energy. See the text for details.